SPATIAL HETERODYNE IMAGING USING A BROADBAND SOURCE

Thesis

Submitted to

The School of Engineering of the

UNIVERSITY OF DAYTON

In Partial Fulfillment of the Requirements for

The Degree of

Master of Science in Electro-Optics

By

James John Zimnicki

Dayton, Ohio

May 2018

SPATIAL HETERODYNE IMAGING USING A BROADBAND SOURCE

Name: Zimnicki, James John

APPROVED BY:

Paul McManamon, Ph. D.
Advisory Committee Chairman
Technical Director, Ladar and Optical Communications Institute (LOCI)
Department of Electro-Optics and Photonics

Ed Watson, Ph.D.
Committee Member
Joint Appointment with University of Dayton Research Institute
Department of Electro-Optics and Photonics

Partha Banerjee, Ph.D.
Committee Member
Chairperson
Department of Electro-Optics and Photonics

Robert J. Wilkens, Ph.D., P.E.
Associate Dean for Research and Innovation
Professor
School of Engineering

Eddy M. Rojas, Ph.D., M.A., P.E.
Dean
School of Engineering

ABSTRACT

SPATIAL HETERODYNE IMAGING USING A BROADBAND SOURCE

Name: Zimnicki, James John
University of Dayton

Advisor: Dr. Paul McManamon

Imaging through obscurants is a critical issue for lidars looking through clouds, or human tissue. Traditionally Spatial heterodyne imaging has been performed with a low-bandwidth laser source that exhibits good coherence length characteristics. One of the drawbacks of using a low-bandwidth source with long coherence length is that signal return from all objects within the coherence length of the source mix equally well on the camera imaging the system. Broadening the bandwidth of the source shortens the coherence length of the system. This thesis intends to show that through careful system design, spatial heterodyne imaging can be performed in the presence of a broadband source, allowing significantly improved imaging in the presence of obscurants such as clouds or human tissue. The method used will be phase modulating the source with a pseudo-random bit sequence and matching the optical path lengths of the signal and local oscillator branches of the system. By matching the path lengths for a pseudo-random coded source we can image objects at specific distances related to the modulation speed and code length, while isolating the power of signal return from objects at other distances as a factor of the autocorrelation coefficient of the code.

ACKNOWLEDGMENTS

I would like to thank my advisor, Dr. Paul McManamon, for giving me so much assistance and insight into devising and writing this thesis. Dr. Jeffrey Kraczek is another who has been such an asset through this research, as well as a good friend.

Thanks is also owed to my fellow classmates in the program, who aided me and helped bounce ideas to fruition.

To the Department of Electro-Optics and Photonics, for helping fund my graduate school, I am deeply grateful.

Lastly, I would like to thank my family and friends who supported me through this process. The long days and the late nights have all been well worth the effort and will hopefully bring greater things to come.

TABLE OF CONTENTS

ABSTRACT iii

ACKNOWLEDGMENTS iv

LIST OF FIGURES vii

LIST OF TABLES ix

CHAPTER 1. INTRODUCTION 1

1.1 Problem Statement 1

1.2 Background 2

1.3 Thesis Overview 2

CHAPTER 2. THEORY 4

2.1 Imaging System 4

2.1.1 Diffraction Theory 4

2.1.2 Transformation from a Lens 7

2.1.3 Imaging 11

2.1.4 Point Source Local Oscillator 14

2.1.5 Off-Axis Digital Holography/Spatial Heterodyne 15

2.2 Temporal Heterodyne Modulation Effects 18

2.2.1 Binary Phase Shift Keying 18

2.2.2 Pseudo-Random Binary Sequence 20

2.2.3 Effects of Phase Mismatch 22

CHAPTER 3. SIMULATION 24

3.1 Spatial Heterodyne System Simulation 24

3.2 Spatial Heterodyne with PRBS Modulation 30
3.3 Spatial Heterodyne with Truncated PRBS Modulation 37
CHAPTER 4. EXPERIMENTAL RESULTS 39
4.1 Lab Setup 39
4.2 Data Collection 43
CHAPTER 5. CONCLUSION 51
5.1 Simulation Conclusion 51
5.2 Experimental Conclusion 51
5.3 Future Work 52
REFERENCES 53
APPENDIX A Spatial Heterodyne Simulation Code (MATLAB) 54

LIST OF FIGURES

Figure 2-1: Diffraction Geometry Showing the Three Planes of Interest: Object, Aperture, and Image 5
Figure 2-2: Thickness Geometry of Lens 8
Figure 2-3: Left: Cropped Region of Fourier Plane Containing Pupil. Right: Fourier Plane Showing Cropped Region 17
Figure 2-4: BPSK Signal (top) and Modulated Carrier Output (bottom) 19
Figure 2-5: Linear Feedback Shift Register 20
Figure 3-1: Slant H Object Used in Simulation 25
Figure 3-2: (a) LO Field with No Added Phase; (b) LO Field with Pi Added Phase 27
Figure 3-3: Fourier Plane from Intensity Image 28
Figure 3-4: Object and LO Fields Retrieved from Fourier Plane 29
Figure 3-5: Intensity of Fields Showing Reconstructed Object Shape 30
Figure 3-6: Object and LO Phase Modulation and Phase Difference w/no Offset 32
Figure 3-7: Object and LO Phase Modulation and Phase Difference w/Less than 1 Bit Offset 33
Figure 3-8: Object and LO Phase Modulation and Phase Difference w/Greater than 1 Bit Offset 33
Figure 3-9: Iterative Loop to Simulate PRBS Modulated System 34
Figure 3-10: Power vs. Standard in Pupil Region in PRBS4 Case 35
Figure 3-11: Power vs. Standard in Pupil Region in PRBS7 Case 36

Figure 3-12: Power vs. Standard in Pupil Region in PRBS9 Case 37
Figure 3-13: Power Isolation from Incomplete Sequences for Various Bit Shifts 38
Figure 4-1: Optical Component Table Layout 40
Figure 4-2: Image of Target Mask; Chrome on Glass Pattern 41
Figure 4-3: Mask Region of Interest 42
Figure 4-4: LabVIEW Panel of Image and Fourier Transform 42
Figure 4-5: Representative Spatial Heterodyne Image Capture 44
Figure 4-6: Fourier/Pupil Plane with No Modulation Applied 44
Figure 4-7: Fourier/Pupil Plane with PRBS7 Modulation Applied 45
Figure 4-8: Recovered Image of “H” Target from Pupil Corresponding to Modulated LO 46
Figure 4-9: Recovered Image of “H” Target from Pupil Corresponding to Unmodulated LO 46

LIST OF TABLES

Table 3-1: Power in Image and from Pupil Region in PRBS4 Case 35

Table 3-2: Power in Image and from Pupil Region in PRBS7 Case 36

Table 3-3: Power in Image and from Pupil Region in PRBS9 Case 36

Table 4-1: Powers from Section of Image with No Modulation 45

Table 4-2: Powers from Sections of Image with PRBS7 Modulation 47

Table 4-3: Powers from Sections of Image with PRBS9 Modulation 47

Table 4-4: dB Isolation Achieved Between Pupils 47

Table 4-5: Powers from Sections of Image with PRBS7 Modulation and 3m Fiber Length 48

Table 4-6: Powers from Sections of Image with PRBS7 Modulation and 9m Fiber Length 48

Table 4-7: Powers from Sections of Image with PRBS7 Modulation and 12m Fiber Length 49

Table 4-8: Isolation Achieved by OPD between Signal and LO Paths 49

CHAPTER 1

INTRODUCTION

1.1 Problem Statement

Spatial heterodyne systems are typically designed using a source laser of high temporal coherence, or coherence length. One drawback of this source is that returns from any distance within the coherence length will mix equally well on the detector array, or camera. Broadening the source linewidth, or bandwidth, has the effect that the coherence length is much shorter and objects at distances greater than this length cannot be imaged clearly.

Just like temporal heterodyne has reduced mixing efficiency when the return signal and the LO are not spatially matched, spatial heterodyne has reduced mixing efficiency when the returned signal and the LO are not temporally matched. Temporal fringes can be created by modulating the phase of either the signal or LO branches of the system, which would cause the spatial fringes on the camera to average over the integration time and wash out, reducing the mixing efficiency. This effect has been shown to have detrimental effects to the sensitivity of the system by creating the appearance of a moving target, and thus, a Doppler shifted signal [1]. The Doppler shift frequency between the signal and LO at the detector create temporal beat frequencies.

By modulating both branches at the same rate we can allow for the relative phase to remain the same, creating stable fringe patterns. In this thesis we show that spatial heterodyne imaging can be performed with a broadband signal. The correct modulation scheme can allow us to reduce the mixing efficiency for areas in the system FOV that are

at distances of no interest, allowing imaging through obscuring media. Pseudo-random bit sequences (PRBS) are such a modulation scheme that will allow us the rejection of interference from distances of no interest.

1.2 Background

Off-axis holography is a field of study that began its existence in 1961 when Leith and Upatnieks[2]–[4] expanded on the work shown by Gabor[5]. With the introduction of the off-axis system, the object field could be disseminated from the image field by a shifting introduced with an off-axis reference beam. This work opened up new opportunities in the field, one of which is the ability to create digital holograms using computers and reconstruction algorithms. Goodman and Lawrence are credited for the first digital hologram in their 1967 paper[6].

The use of PRBS are well known in the communications and radar communities. The work by MacWilliams and Sloane has summarized the properties of such sequences[7]. The property of interest to the process of spatial heterodyne imaging is the autocorrelation rejection for misaligned codes, those delayed in return time at the detector. This property is still being explored in recent works[8], [9] for various heterodyne applications and shows the potential to work in a coherent imaging system as well.

1.3 Thesis Overview

Chapter 2 of this thesis consists of imaging theory for a spatial heterodyne system as well as theory for the effects of modulation in creating temporal fringes. We describe how pseudo-random bit sequence can be used to align our code to specific distances and the amount of isolation provided by a misalignment of the code. Chapter 3 will discuss the simulation of the system in the MATLAB environment involving a few different codes and their effects on the system. The effect of incomplete code sequences is also discussed.

Chapter 4 will cover the lab experiment implementing the theory and system design covered by this thesis and will show how it can operate in practice. Chapter 5 will discuss the results of each section and conclude with a recommendation of future work in this area.

CHAPTER 2

THEORY

2.1 Imaging System

In this section we develop the imaging system diffraction theory relevant to our project. Both the work by Goodman[10] and Kraczek[11] will be used as it applies to this thesis. We start with the diffraction of an object through a space and a single lens and then develop the theory behind spatial heterodyne systems.

2.1.1 Diffraction Theory

In order to describe the effects of the phase modulation on the spatial heterodyne process, diffraction effects in the system must first be defined. The general starting point for diffraction theory is the Huygens-Fresnel principle, which is rewritten in Goodman[10], equation 4-9, as shown in Equation 2.1.

$$U(x,y) = \frac{z}{j\lambda}\iint_{\Sigma} U(\xi,\eta)\frac{\exp(jkr)}{r^2}\,d\xi\,d\eta \tag{2.1}$$

This defines the diffraction of a point in the object plane, $U(\xi, \eta)$, into the secondary plane which we will call the aperture plane, U(x, y). A depiction of the space is shown in Figure 2-1 below.

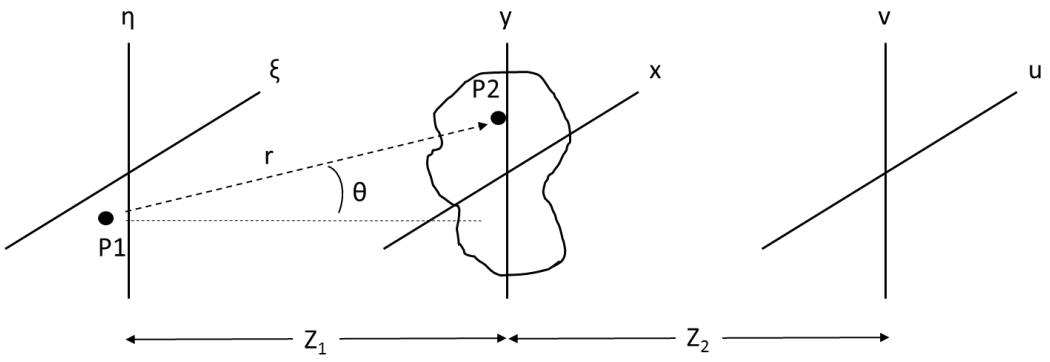

Figure 2-1: Diffraction Geometry Showing the Three Planes of Interest: Object, Aperture, and Image

As shown in the illustration, *r* is the distance between the point P_1 in the object plane and P_2 in the aperture plane. This distance can be shown to be

$$r = \sqrt{{z_1}^2 + (x-\xi)^2 + (y-\eta)^2}\,, \tag{2.2}$$

which is simply the distance formula between two points in rectangular coordinates.

The Huygens-Fresnel principle can be reduced to a simpler form to aid in the analysis of our optical system, called the Fresnel diffraction integral. This will give an approximation in the near field of the object. In order to build this approximation, we first look at the equation for *r*, Eq. (2.2), and factor out the z_1 term from the radical expression

$$r = z_1\sqrt{1 + \left(\frac{(x-\xi)}{z_1}\right)^2 + \left(\frac{(y-\eta)}{z_1}\right)^2}\,. \tag{2.3}$$

From Eq. (2.2) it can be shown, as in Goodman, that we can use the binomial expansion of the square root term in order to obtain a good approximation of the distance *r* between P_0 and P_1. The radical term can then be viewed as

$$\sqrt{1+b} = 1 + \frac{1}{2}b + \frac{1}{8}b^2 + \cdots, \tag{2.4}$$

of which we will take only the first two terms. This is appropriate if the magnitude of $z_1 \gg (x-\xi)\ or\ (y-\eta)$, which will be assumed for our system and shown later to be accurate.

Using the first two terms of Eq. (2.4) where $b = \left(\frac{(x-\xi)}{z_1}\right)^2 + \left(\frac{(y-\eta)}{z_1}\right)^2$, we reduce Eq. (2.3) to

$$r \approx z_1\left[1+\frac{1}{2}\left(\frac{x-\xi}{z_1}\right)^2+\frac{1}{2}\left(\frac{y-\eta}{z_1}\right)^2\right], \tag{2.5}$$

which we substitute into Eq. (2.1) to get

$$U(x,y) = \frac{z_1}{j\lambda}\iint_{-\infty}^{\infty} U(\xi,\eta)\frac{\exp\left(jkz_1\left[1+\frac{1}{2}\left(\frac{x-\xi}{z_1}\right)^2+\frac{1}{2}\left(\frac{y-\eta}{z_1}\right)^2\right]\right)}{\left(z_1\left[1+\frac{1}{2}\left(\frac{x-\xi}{z_1}\right)^2+\frac{1}{2}\left(\frac{y-\eta}{z_1}\right)^2\right]\right)^2}\,d\xi\,d\eta\,. \tag{2.6}$$

.

To simplify Eq. (2.6) we can assume that the contributions from the *r* term we substituted into the bottom of the quotient to be negligible apart from the lone z_1 term that results from the product. For the exponential term the same cannot be said, as if we assume our system to have a wavelength $\lambda \approx 0.5\,\mu m$, our wavenumber is on the order of $10^7\ m^{-1}$. This fact, combined with the knowledge that phase wraps at 2π, means that we cannot make such an assumption as we did with the quotient term.

Eq. (2.6) then reduces to

$$U(x,y) = \frac{z_1}{j\lambda}\iint_{-\infty}^{\infty} U(\xi,\eta)\frac{\exp\left(jkz_1\left[1+\frac{1}{2}\left(\frac{x-\xi}{z_1}\right)^2+\frac{1}{2}\left(\frac{y-\eta}{z_1}\right)^2\right]\right)}{\left(z_1\left[1+\frac{1}{2}\left(\frac{x-\xi}{z_1}\right)^2+\frac{1}{2}\left(\frac{y-\eta}{z_1}\right)^2\right]\right)^2}\,d\xi\,d\eta\,, \tag{2.7}$$

and redistributing the top exponential we come to Eq. (2.7)

$$U(x,y) = \frac{1}{j\lambda z_1}\iint_{-\infty}^{\infty} U(\xi,\eta)\exp\left(jkz_1+\frac{jk}{2z_1}(x-\xi)^2+\frac{jk}{2z_1}(y-\eta)^2\right)d\xi\,d\eta\,, \tag{2.8}$$

which further reduces, again, to

$$U(x,y) = \frac{e^{jkz_1}}{j\lambda z_1} \iint_{-\infty}^{\infty} U(\xi,\eta) \exp\left(\frac{jk}{2z_1}[(x-\xi)^2 + (y-\eta)^2]\right) d\xi \, d\eta \,. \qquad (2.9)$$

Eq. (2.9) is the Fresnel diffraction integral that we were interested in developing from the Huygens-Fresnel principle. This equation defines the diffracted field at coordinate (*x*, *y*) given a field from the (*ξ*, *η*) plane.

For ease in later calculations, we introduce the Point Spread Function (PSF) which defines the impulse response of our system to a single point object. We start with a delta function, defined at a point *(ξ_0, η_0)* in the object plane, as

$$U(\xi,\eta) = \delta(\xi - \xi_0, \eta - \eta_0) \,. \qquad (2.10)$$

We then insert this function into Eq. (2.9) and evaluate it to get the result

$$U_l(x,y) = \frac{e^{jkz_1}}{j\lambda z_1} \, e^{\frac{jk}{2z_1}[(x-\xi_0)^2 + (y-\eta_0)^2]} \,. \qquad (2.11)$$

If we want to generalize for any point in the object plane, we can change *(ξ_0, η_0)* simply to *(ξ, η)* to get

$$U_l(x,y) = \frac{e^{jkz_1}}{j\lambda z_1} \, e^{\frac{jk}{2z_1}[(x-\xi)^2 + (y-\eta)^2]} \,. \qquad (2.12)$$

This defines the field contribution in the aperture plane by a single point in the object plane, and will need the combinations of all points in the object plane to create the total field incident in the aperture plane.

2.1.2 Transformation from a Lens

For our experiment we will be using a simple, single-lens imaging system. For simplicity, we assume our lens to be a perfect thin lens. If we look at the geometry of a lens, as drawn in Goodman[10], we see what is shown in Figure 2-2.

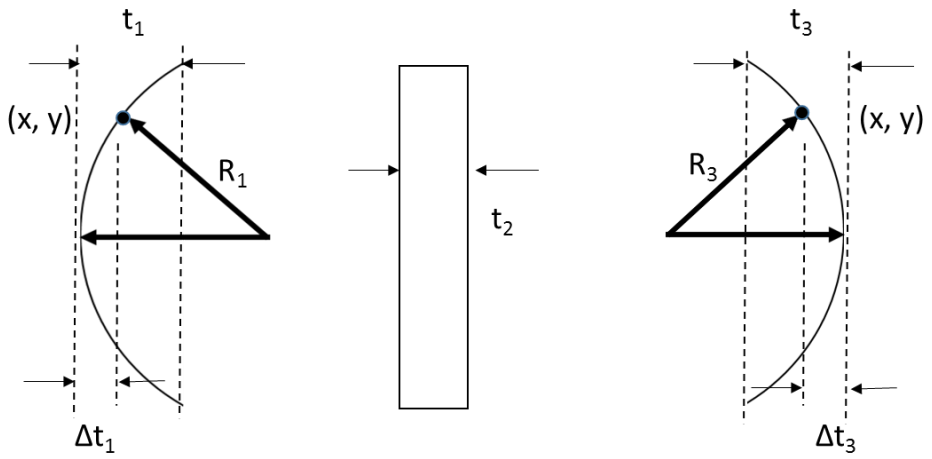

Figure 2-2: Thickness Geometry of Lens

In Figure 2-2 we have several terms to define. Each section of the lens has an overall thickness designated by t_n where n corresponds to the section number. For the first and third sections, we have the terms R_n and Δt_n, which are the radius of the lens and the distance travelled before coming into contact with the lens surface, respectively. At the lens' widest point along the optical axis Δt_n, would equal 0, whereas at a point (x, y) it would equal either

$$\Delta t_1 = R_1 - \sqrt{R_1^2 - x^2 - y^2} \tag{2.13}$$

or

$$\Delta t_3 = -R_3 - \sqrt{R_3^2 - x^2 - y^2} \tag{2.14}$$

dependent on which section of the lens is being analyzed. We ignore the flat, middle section of the lens because we assume a perfect thin lens, but this would result in a constant thickness/phase term.

The total thickness of each section at a point (x, y) is then simply the subtraction of the Δt_n term from the t_n term in each region, and is given in Eqs. (2.15) & (2.16).

$$\Delta_1(x,y) = t_1 - \left[R_1 - \sqrt{R_1^2 - x^2 - y^2}\right] \tag{2.15}$$

$$\Delta_3(x,y) = t_3 - \left[-R_3 - \sqrt{R_3^2 - x^2 - y^2}\right] \tag{2.16}$$

The total thickness of the lens at the point (*x, y*) can then be expressed as

$$\Delta(x,y) = t - R_1\left[1 - \sqrt{1 - \frac{x^2+y^2}{{R_1}^2}}\right] + R_3\left[1 - \sqrt{1 - \frac{x^2+y^2}{{R_3}^2}}\right], \tag{2.17}$$

where $t = t_1 + t_3$. This is similar to the result Goodman[10] reaches in Eq. (5-6) of his text, although we've ignored the central section of the lens.

The thickness function in Eq. (2.17) can be simplified further if we use a paraxial ray assumption, that is, that only the wavefront nearest the optical axis is of interest. This is easily made in practice and in our single lens imaging system (4f system) by using a reasonably small lens with a long focal length, or, consequently, that the radius of the lens is large in comparison with the off-axis distance of our point. When we make this assumption, we can use a Taylor series expansion to get

$$\Delta t_n(x,y) = R_n\left[1 - \sqrt{1 - \frac{x^2+y^2}{{R_n}^2}}\right] \approx R_n\left[1 - \left(1 - \frac{x^2+y^2}{{R_n}^2}\right)\right] = \frac{x^2+y^2}{2R_n} \tag{2.18}$$

Eq. (2.18) is then easily substituted into Eq. (2.17) to give

$$\Delta(x,y) = t - \frac{x^2+y^2}{2R_1} + \frac{x^2+y^2}{2R_3} = t - \frac{x^2+y^2}{2}\left(\frac{1}{R_1} - \frac{1}{R_3}\right), \tag{2.19}$$

Having the thickness function of the lens, we then want to find the phase change it causes. Phase change is accumulated in a medium as

$$\Phi = \frac{2\pi}{\lambda} nL = knL\,, \tag{2.20}$$

where n is the refractive index of the medium, L is the distance travelled in the medium and k is the wavenumber. If we are to find the phase accumulation travelling through a portion of the lens at a point (x, y), we must describe each section of the lens with phase. The first section accumulates a phase of

$$\Phi_1(x,y) = k(n_l(t_1 - \Delta t_1(x,y) + n_a \Delta t_1(x,y)), \tag{2.21}$$

where n_l is the refractive index of the lens and n_a is that of air.

We continue to ignore the second section and describe the third section as

$$\Phi_3(x,y) = k(n_l(t_3 - \Delta t_3(x,y) + n_a \Delta t_3(x,y)), \tag{2.22}$$

and since we know our simplified equation for Δt_n, the phase accumulation is then

$$\Phi_n(x,y) = k\left(n_l\left[t_n - \frac{x^2+y^2}{2R_n}\right] + n_a\frac{x^2+y^2}{2R_n}\right), \tag{2.23}$$

or

$$\Phi_n(x,y) = k\left(n_l t_n + (n_a - n_l)\frac{x^2+y^2}{2R_n}\right). \tag{2.24}$$

We can now add the contributions to phase change by the two interesting sections of the lens, which results in

$$\Phi_l(x,y) = \Phi_1(x,y) + \Phi_3(x,y) = \tag{2.25}$$
$$k\left(\left(n_l t_1 + (n_a - n_l)\frac{x^2+y^2}{2R_1}\right) + \left(n_l t_3 + (n_a - n_l)\frac{x^2+y^2}{2R_3}\right)\right) =$$
$$kn_l(t_1+t_3) - k\frac{(x^2+y^2)}{2}\left[(n_l - n_a)\left(\frac{1}{R_1} - \frac{1}{R_3}\right)\right].$$

Looking at the last bracketed term in Eq. (2.25) we notice a familiar equation. As Goodman notes, this term can be combined into a common term f, and is a form of the commonly known lens-marker's formula.

$$\frac{1}{f} = (n_l - 1)\left(\frac{1}{R_1} - \frac{1}{R_3}\right). \tag{2.26}$$

We have simplified our form of the lens-maker's formula by assuming n_a to be that of air, or ≈1. Then simplifying Eq. (2.25) with this step we get to

$$\Phi_l(x,y) = kn_l t - k\frac{(x^2+y^2)}{2f}. \tag{2.27}$$

This result leads to the change in the field due to the lens, which is given as

$$U_{lens} = e^{jknt}P(x,y)e^{\left(-j\frac{k}{2f}(x^2+y^2)\right)}, \tag{2.28}$$

where *P(x, y)* is the extent of the lens in space and is referred to as the pupil function.

$$P(x,y) = \begin{cases} 1\ inside\ the\ extent\ of\ lens \\ 0\ elsewhere \end{cases} \tag{2.29}$$

To find the field behind the lens we multiply Eq. (2.28) by Eq. (2.12) to get

$$U_l{}'(x,y) = e^{jknt}U_l(x,y)P(x,y)e^{\left(-j\frac{k}{2f}(x^2+y^2)\right)}, \tag{2.30}$$

which is the same result found in Goodman, Eq. 5-12, apart from the constant phase factor which is ignored in his text.

2.1.3 Imaging

The last piece of Figure 2-1 left to discuss is the formation of the image as the field propagates from the aperture plane to the image plane. To describe this section we recycle the derivation for Eq. (2.9) and simply shift the coordinate planes of interest.

$$U(u,v) = \frac{e^{jkz_2}}{j\lambda z_2}\iint_{-\infty}^{\infty} U_l'(x,y)e^{\left(\frac{jk}{2z_2}[(u-x)^2+(v-y)^2]\right)}\,dx\,dy \tag{2.31}$$

We can now describe the propagation through the system as the combination of Eqs. (2.31), (2.30), and (2.12). First, Eq. (2.31) should now be reclassified as the impulse response, that is, the function that describes the relationship between a point-source at the object plane and its field in the output, or image, plane. As Goodman notates in Eq. 5-24, the impulse response, *h*, should be approximately a Dirac delta function, plus or minus any magnification, *M*, or a constant phase term, *K*.

$$h(u,v;\ \xi,\eta)\ \approx K\ \delta(u\ \pm M\xi, v\ \pm M\eta) \tag{2.32}$$

We rewrite and simplify to get Eq. (2.33).

$$h(u,v;\xi,\eta) = \frac{1}{\lambda^2 z_1 z_2} e^{jk(z_1+z_2)} e^{jknt} e^{\frac{jk}{2z_2}(u^2+v^2)} e^{\frac{jk}{2z_1}(\xi^2+\eta^2)} \iint_{-\infty}^{\infty} P(x,y) e^{j\frac{k}{2}\left(\frac{1}{z_1}+\frac{1}{z_2}-\frac{1}{f}\right)(x^2+y^2)} e^{\left(-jk\left[\left(\frac{\xi}{z_1}+\frac{u}{z_2}\right)x+\left(\frac{\eta}{z_1}+\frac{v}{z_2}\right)y\right]\right)}\, dx\, dy\ . \tag{2.33}$$

To eliminate some of the terms in Eq. (2.33) and simplify it significantly, we can now make some assumptions as to the quadratic phase terms. Starting with the term $e^{\frac{jk}{2z_2}(\xi^2+\eta^2)}$, we assume that the distance from the object to the lens is much greater than the physical size of the object, and so the term equals unity.

The second term to consider is in the integral, $e^{j\frac{k}{2}\left(\frac{1}{z_1}+\frac{1}{z_2}-\frac{1}{f}\right)(x^2+y^2)}$, and can be ignored if we use the lens law so that imaging takes place, that is $\left(\frac{1}{z_1}+\frac{1}{z_2}-\frac{1}{f}\right)=0$.

The third term, $e^{\frac{jk}{2z_2}(u^2+v^2)}$, cannot be ignored because we neither measure the field of the image on a spherical surface nor do we ignore the phase distribution of the image. Since we have eliminated two of the three quadratic phase terms, we rewrite Eq. (2.33) as

$$h(u,v;\xi,\eta) = \tag{2.34}$$

$$\frac{1}{\lambda^2 z_1 z_2} e^{jk(z_1+z_2)} e^{jknt} e^{\frac{jk}{2z_2}(u^2+v^2)} \iint_{-\infty}^{\infty} P(x,y) e^{\left(-jk\left[\left(\frac{\xi}{z_1}+\frac{u}{z_2}\right)x+\left(\frac{\eta}{z_1}+\frac{v}{z_2}\right)y\right]\right)} dx\, dy \ .$$

We then rewrite Eq. (2.34) taking into account the magnification factor $M = -\frac{z_2}{z_1}$ as,

$$h(u,v;\xi,\eta) = e^{jk(z_1+z_2)} e^{jknt} e^{\frac{jk}{2z_2}(u^2+v^2)} \frac{M}{\lambda^2 {z_2}^2} \iint_{-\infty}^{\infty} P(x,y) e^{\left(-\frac{jk}{z_2}[(u-M\xi)x+(v-M\eta)y]\right)} dx\, dy \ . \quad (2.35)$$

Ignoring the magnification term, as we set it to be negative unity, we see that the integral of Eq. (2.35) is a Fourier transform of *P(x,y)*.

$$h(u-\xi, v-\eta) = e^{jk(z_1+z_2)} e^{jknt} e^{\frac{jk}{2z_2}(u^2+v^2)} \frac{M}{\lambda^2 {z_2}^2} \mathcal{F}[P(x,y)] \Big|_{fx=\frac{u+\xi}{\lambda z_2}, fy=\frac{v+\eta}{\lambda z_2}} \quad (2.36)$$

Since we know the impulse response of the system, Goodman states that we can write the image field U_i as he states in Eq. 5-23,

$$U_i(u,v) = \iint_{-\infty}^{\infty} h(u,v;\xi,\eta) U_o(\xi,\eta) d\xi d\eta \ . \quad (2.37)$$

This equation states that the image field can be described as the point responses of individual samples of the object field $U_o(\xi,\eta)$. Since we have already described the point response function of our system, we can now describe the image field as

$$U_i(u,v) = e^{jk(z_1+z_2)} e^{jknt} \frac{M e^{\frac{jk}{2z_2}(u^2+v^2)}}{\lambda^2 {z_2}^2} \iint_{-\infty}^{\infty} U_o(\xi,\eta) \mathcal{F}[P(x,y)] \Big|_{fx=\frac{u+\xi}{\lambda z_2}, fy=\frac{v+\eta}{\lambda z_2}} d\xi d\eta \quad (2.38)$$

2.1.4 Point Source Local Oscillator

In order to create the spatial heterodyne imaging we mix the input field with a local oscillator that will create the spatial fringes across the detector surface. The local oscillator (LO) used will be from a fiber tip, as this closely approximates a point source, to create a spherical wave front within the numerical aperture of the fiber To create stationary fringes the LO and signal need to be the same wavelength (which can be done by using the same laser) and the difference in the object and LO optical paths need to be within the coherence length of the laser. We will discuss optical path length in another section.

We model a point source as a Dirac delta function. We shift the delta function from the axis which, as we will later show, causes a separation between the LO and the pupil field terms in the Fourier plane. The equation we use for the delta function is

$$U(\alpha,\beta) = \delta(\alpha-\alpha_0,\beta-\beta_0), \tag{2.37}$$

as written by Kraczek[11], Eq. 2.54 in his thesis.

As is done in his text, we diffract the LO to the image plane in a similar fashion to what was done previously.

$$U(u,v) = \frac{e^{jkz_3}}{j\lambda z_3}\iint_{-\infty}^{\infty} U(\alpha,\beta)\exp\left(\frac{jk}{2z_3}[(u-\alpha)^2+(v-\beta)^2]\right)\,d\alpha\,d\beta\,. \tag{2.38}$$

where z_3 is a new distance, defined as the distance from the LO source to the image plane. Just as before, we expand Eq. (2.38) to

$$U(x,y) = e^{\frac{jk}{2z_3}(u^2+v^2)}\,\frac{e^{jkz_3}}{j\lambda z_3}\iint_{-\infty}^{\infty}\delta(\alpha-\alpha_0,\beta-\beta_0)e^{\frac{-jk}{z_3}(u\alpha+v\beta)}e^{\frac{jk}{2z_3}(\alpha^2+\beta^2)}\,d\alpha\,d\beta\,. \tag{2.39}$$

Eq. (2.39) is evaluated as

$$U_{LO}(x,y) = \frac{e^{jkz_3}}{j\lambda z_3}e^{\frac{jk}{2z_3}(u^2+v^2)}\,e^{\frac{-jk}{z_3}(u\alpha_0+v\beta_0)}e^{\frac{jk}{2z_3}({\alpha_0}^2+{\beta_0}^2)}\,. \tag{2.40}$$

In order to create a regular spatial fringe pattern we must match the quadratic terms of the LO and signal. If the two are unmatched the fringe pattern will vary in spatial frequency as a function of the position on the detector; the fringes cannot be sampled if they become smaller than the Nyquist frequency of the pixels.

To mode match the LO to the signal we write

$$e^{\frac{jk_S}{2z_2}(u^2+v^2)} = e^{\frac{jk_{LO}}{2z_3}(u^2+v^2)}. \tag{2.41}$$

We can solve for the condition of mode matching our point source LO as

$$z_3 = \frac{z_2\lambda_s}{\lambda_{LO}}. \tag{2.42}$$

In Kraczek[11], z_2 is written as f_s, or the focal length of the lens for the signal. We write z_2 due to the nature of our 4f system, or equivalently $2f_s$. Since this is the case, our LO must be in the same plane as the lens for mode matching to occur.

2.1.5 Off-Axis Digital Holography/Spatial Heterodyne

Camera sensors are not quick enough to follow the phase of incident light. Since we are unable to collect the amplitude and phase information of the field directly, we must resort to mathematically extracting it. Fortunately, systems exist that allow us to image an object and determine its phase information using post-processing. One such technique is off-axis holography, or spatial heterodyne. As its name implies, this system uses an off-axis signal, the LO in this case, in order to provide separation between the signal and the reference wave during the analytics.

Mixing the signals onto the camera detector gives us the intensity of the combined fields, expressed as

$$|U_s + U_{lo}|^2 = |U_s|^2 + |U_{lo}|^2 + U_s U_{lo}^* + U_s^* U_{lo} \tag{2.43}$$

In order to separate the fields from each other, we first take the Fourier transform of the image. The purpose of this transform is to separate the fields in the Fourier plane. We call this space the pupil plane because it contains the physical shape of our pupil, but also contains the LO beams which are outside of the physical pupil space. The Fourier transform of Eq. (2.43) is

$$\mathcal{F}\{|U_s + U_{lo}|^2\} = \mathcal{F}\{|U_s|^2\} + \mathcal{F}\{|U_{lo}|^2\} + \mathcal{F}\{U_s U_{lo}{}^*\} + \mathcal{F}\{U_s{}^* U_{lo}\}. \quad (2.44)$$

The two terms of interest are the last two in Eq. (2.44), which are conjugate terms of the product of the signal and LO fields. Since the Fourier transform separates the terms in space due to the angle between the LO and object signal, we can crop out the terms we are interested in, effectively eliminating the rest, as depicted in Figure 2-3. The separation between the LO and signal source is the $e^{\frac{jk}{2z_3}(u\alpha_0 + v\beta_0)}$ term from our point source LO (Eq. 2.40). This tilt term transforms to a translation of the pupil field in the Fourier plane. Re-centering the pupil in the new crop eliminates the tilt term when transformed back to the image plane, where we have the desired field's amplitude and phase. The system is modeled by the Eq. (2.45), in which we say that taking the inverse Fourier transform of the cropped region of interest, we obtain the fields of interest.

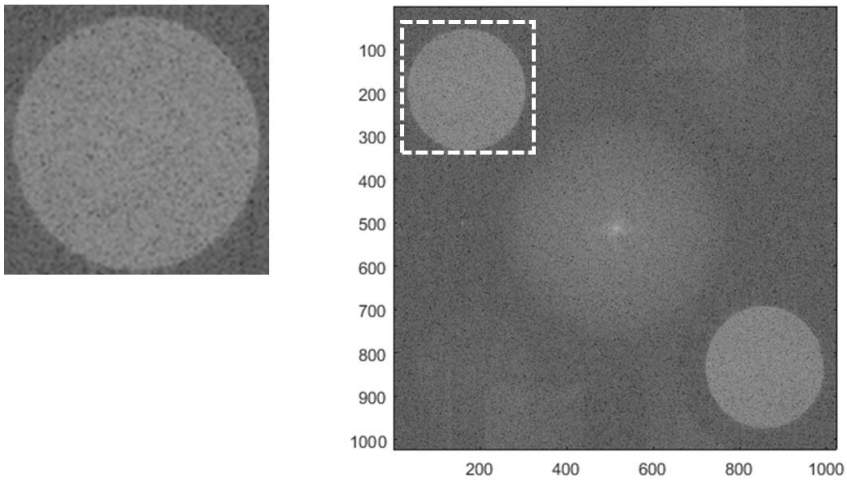

Figure 2-3: Left: Cropped Region of Fourier Plane Containing Pupil. Right: Fourier Plane Showing Cropped Region

$$U(u,v) = \mathcal{F}^{-1}\{\mathcal{F}\{U_s {U_{lo}}^*\}\} = U_s(u,v)U_{lo}(u,v)^*. \tag{2.45}$$

We rewrite Eq. (2.40) with the removed tilt term and add in the temporal component that will help us later,

$$U_{LO}(x,y) = \frac{e^{jkz_3}}{j\lambda z_3} e^{\frac{jk}{2z_3}(u^2+v^2)}\, e^{\frac{jk}{2z_3}({\alpha_0}^2+{\beta_0}^2)} e^{-j(\omega_{LO}t+\varphi_{LO})}. \tag{2.46}$$

We can do the same for the signal field U_i to obtain U_s, which we write simply,

$$U_s(u,v) = U_i(u,v)e^{-j(\omega_S t+\varphi_S)}. \tag{2.47}$$

Eqs. (2.46) & (2.47) allow us to show the effects that a temporal mismatch can have on our imaging by writing Eq. (2.45) as

$$U(u,v) = \left[U_s(u,v)e^{j(\omega_S t+\varphi_S)}\right]\left[U_{lo}(u,v)^* e^{-j(\omega_{LO}t+\varphi_{LO})}\right]. \tag{2.48}$$

From Eq. (2.48) we see that if the frequencies of the signal beam and LO match the result is the field of interest with an added constant phase term. Whether or not the phases

match is of little concern because the difference will be a constant; however, when the phases are modulated it becomes an issue if the phases change at a different rate.

2.2 Temporal Heterodyne Modulation Effects

This section will explore the effects of phase modulation on our spatial heterodyne system and how it creates a temporal component when mismatched between the signal and LO legs of the system. We will first explain the technique of binary phase shift keying (BPSK). Later we will develop the idea further using PRBS.

2.2.1 Binary Phase Shift Keying

The modulation technique used in this experiment will be BPSK, chosen because it allows us to use a relatively simple system by which to achieve our goal of range gating, where higher-order PSK modes are useless because they are strictly meant for higher data rates in communication channels. BPSK uses two phases, as its name implies, to shift the carrier signal by 180° or π. This can be illustrated in Figure 2-4 where we see the phase of the carrier instantaneously changed due to the modulation signal.

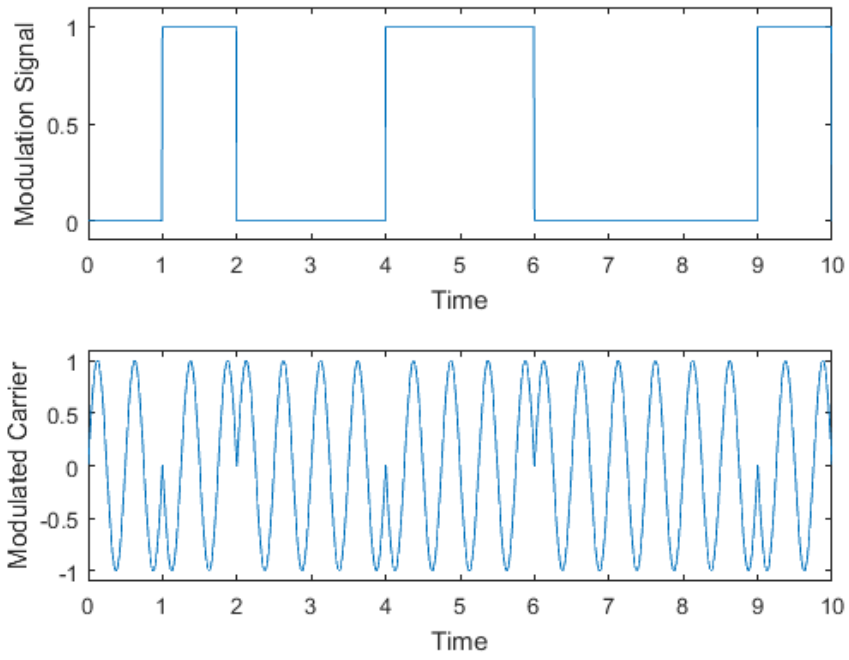

Figure 2-4: BPSK Signal (top) and Modulated Carrier Output (bottom)

We see in Figure 2-4 that our signal's effect on the carrier waveform is that of instantly reversing its phase, or effectively inverting the waveform since we use a pi phase shift. In the example illustrated, the phase reversals occur at the zero crossings of the carrier, but this is not at all necessary in our final system and would be, in fact, very difficult to achieve at optical frequencies.

The modulation effect of BPSK can be simply described as

$$S(0) = A * e^{j*0} \qquad (2.49)$$
$$S(1) = A * e^{j*\pi},$$

where *S(b)* indicates the output for a given binary input. We have written that a "1" represents a pi phase shift, but this is not absolute and depends on the convention being used.

2.2.2 Pseudo-Random Binary Sequence

To identify how a PRBS is useful, we should first understand how it is created. The sequence is generated by linear feedback shift-registers (LFSR), or a system of devices that feeds the output of the previous state into the input of the next state. This system is shown in Figure 2-5.

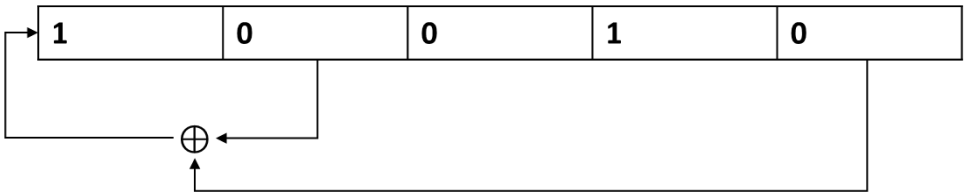

Figure 2-5: Linear Feedback Shift Register

This depiction shows how a LFSR might be structured as a circuit, where the $\oplus$ symbol indicated a "XOR" gate. The output of this circuit is the right-most bit and the next state is generated by taking the feedback nodes and passing them to the input shifting the remaining bits right. The feedback nodes indicate what is known as the feedback or characteristic polynomials. The right-most indicates the highest order of the polynomial, in this case x^5, and the input bit is always x^1. The x^0 term is present in the polynomial equation, but is not indicated by a tap. The LFSR depicted in Figure 2-5 would be written as $x^5 + x^2 + 1$.

This same polynomial is special because it is also a maximum length sequence (MLS) polynomial. Since we have a LFSR of 5 bits, the MLS that can be generated is given by

$$N = 2^k - 1. \tag{2.50}$$

The sequence length is given as N and k is the number of shift-registers. The 5 bit system would then have a MLS of N = 31. Not all polynomials representing the feedback taps will generate a MLS. All MLS' will have the property that if a window k bits wide is slid

across the sequence all possible “words” will be generated within the sequence, except for the “null” term of all zeros, which would lead to a halted state because the device could never generate the next state successfully.

Each MLS contains identical frequency content, being comprised of the same words, regardless of the order in which they appear in the sequence. A PRBS will also have the autocorrelation property of

$$r(i) = \begin{cases} 1 \ for \ i = 0 \\ -\frac{1}{N} \ for \ 1 \leq |i| \leq N-1 \end{cases} \tag{2.51}$$

which says that the autocorrelation peak occurs at an offset of 0 bits and any integer of bits offset from that will experience an autocorrelation factor proportional to the length of the sequence[7]. Obviously then, it is useful in communications or telemetry, where applying this code to a waveform gives a very definite offset position to a waveform, something exploited in GPS. This is the property we are interested in exploring in this thesis.

The coherence length of a system is generally given by the equation

$$L = \frac{c}{\Delta \nu}, \tag{2.52}$$

where c is the speed of light and Δv is the linewidth, or bandwidth, of the source. This equation is modified with a change in the refractive index of the medium, but we assume that to be unity for the purposes of this thesis, as it has little effect to us.

Physically, as the PRBS travels through space it has length features related to its pattern length and modulation frequency. The bit rate, or modulation frequency, determines the temporal duration of each bit as well as the spatial extent, and so we modify Eq. (2.52) as,

$$L_b = \frac{c}{bit \ rate} \tag{2.52}$$

where L_b is the length is meters and c is the speed of light. We will also relate this our alignment length, which is a fraction of the length of the bit.

The total length of the code is then

$$L_c = L_b * N \tag{2.53}$$

or, the bit length multiplied by the code length. If we reach the repetition length, the PRBS will once again have a correlation factor of unity. For this reason it is important to have a longer bit sequence for long depths of field being imaged as well as for high modulation rates.

2.2.3 Effects of Phase Mismatch

As we have described above, adding a phase code to the signal or LO beam in our spatial heterodyne system can have a great effect to the process. If we once again look at Eq. (2.48), written again here for reference, we see that a constant phase difference between the two terms makes no difference overall. This is what allows us to perform spatial heterodyne imaging on stationary objects easily.

$$U(u,v) = \left[U_s(u,v)e^{j(\omega_S t+\varphi_S t)}\right]\left[U_{lo}(u,v)^* e^{-j(\omega_{LO} t+\varphi_{LO} t)}\right]. \tag{2.48}$$

If we begin to change the phase of one of the fields relative to the other we create a temporal phase component and the terms no longer cancel. The shift in the relative phase causes the fringe pattern at the image plane to average and wash out, making the process less efficient the more the phase is modulated.

However, if we modulate the two fields at the same rate and with the same waveform at the image plane the phase remains constant and the fringes on the detector stay stationary. An important factor in considering the system's physical structure will then be the optical path length from the electro-optic phase modulator to the image plane. The optical path length for a medium of constant refractive index is given as

$$OPL = n * d \tag{2.54}$$

where *n* is the index of refraction of the medium and *d* is the distance travelled through the medium. In order to maintain the phase relation between our signal and LO the optical path length difference between the two should be either zero or a multiple of L_c, the length of the code in space.

CHAPTER 3

SIMULATION

3.1 Spatial Heterodyne System Simulation

This section will cover the necessary steps to reproduce a spatial heterodyne system in simulation, using MATLAB. We will take portions of the theory developed in the previous chapter and make assumptions in order to simplify the simulation calculation load. The goal of this section is to lay the foundation on which to build the phase modulation technique.

We begin by recalling Eq. (2.43), which describes the intensity pattern on the camera as the modulus square of signal and LO fields.

$$|U_s + U_{lo}|^2 = |U_s|^2 + |U_{lo}|^2 + U_s U_{lo}{}^* + U_s{}^* U_{lo} \tag{2.43}$$

In order to combine these fields we must first create them in MATLAB.

The first term, the signal is easily modeled. We recall earlier that we stated the image field in a geometric optical model can be described as the impulse response of the system convolved with a magnified, inverted field of the object with a constant phase factor applied through its propagation. For our simulation and experiment we assume no magnification, and the image inversion can be ignored for our purposes. Starting with an image of our target, as depicted in Figure 3-1, what we see is the intensity pattern, therefore taking the square root of the object components will give us a pseudo-field to start with. We could add a random phase term to the object's field, but since we are not concerned with static phases, we need not trouble with this step.

The object we use is a slant “H” portion of an ISO12233 target, typically used for MTF reports. It is the portion of the chrome on glass target used in our lab experiment. A “.png” graphic file was created to simulate the binary shaded shape, shown in Figure 3-1.

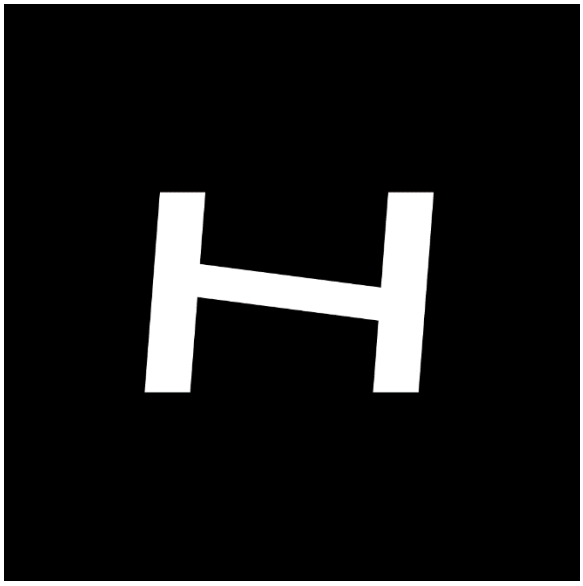

Figure 3-1: Slant H Object Used in Simulation

The impulse response of the system can be modeled by taking the Fourier transform of the lens pupil, as it was stated in Goodman to be a special case of the Fraunhofer diffraction pattern in our system. Having this result we can convolve it with our object field to get the image field. A simpler and quicker operation in MATLAB would be to instead take the individual Fourier transforms, multiply, and then inverse transform back, as stated in Eq. (2.55).

$$U_i(u,v) = \tilde{h}(u,v) \otimes U_g(u,v) = \mathcal{F}^{-1}\{\mathcal{F}(\tilde{h}) \cdot \mathcal{F}(U_g)\} \tag{2.55}$$

The periodicity of the Fourier transform shows that two forward transforms yields a reversed image. Using this property, we can assume that a double forward transform on a circular binary mask would not change the mask; we simply need to transform the object field and multiply the two fields. This simplifies the computational step immensely.

The LO term takes more effort to model in the imaging plane, as we need to propagate a point source from the pupil plane. We use Eq. (2.40) which gives the Fresnel diffraction pattern of the point source LO shifted in space. To calculated the shift for the α and β terms take the pixel pitch resolution which is $\frac{1}{5.86\ \mu m} = 170.648\ mm^{-1}$. By Nyquist's theorem, we can only sample spatial frequencies of half that, or $85.324\ mm^{-1}$. The angle between the LO and the optical axis is roughly

$$\sin\theta = \frac{x}{2\ m}, \tag{3.1}$$

where *x* is the spacing between the LO and the axis, and 2 meters is roughly the length of the hypotenuse.

Since the propagation distance to the camera is much greater than the diameter of the sensor, we can assume a nearly planar, tilted wavefront, the spatial frequency given as

$$\alpha \approx \frac{\sin\theta}{\lambda}. \tag{3.2}$$

Solving for the ***sinθ*** term and setting it equal to Eq.(3.1), we find that $x = 2 * \alpha * \lambda$, or that the maximum shift we can have before undersampling is about 9.08 cm, or 3.57 in from the optical axis.

As we then have our spatial variables defined, we iteratively find the field of the LO at the image plane by solving for the amplitude and phase at each point in the plane. This gives a phase distribution based on the real portion of the field, as shown in Figure 3-2.

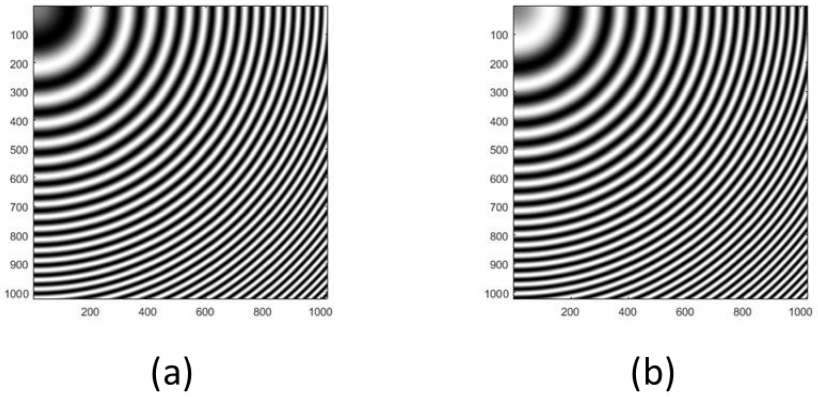

Figure 3-2: (a) LO Field with No Added Phase; (b) LO Field with Pi Added Phase

These two fields represent the LO with either 0 or pi phase shift added to it. These are not the actual fields used in the simulation, but are shifted closer to the optical axis to show the detail of the fringes better as the phase is shifted. Since we are only modulating the phase by these two states, we need to only generate these fields once for the remainder of the simulation.

After we have the fields of the object and the LO at the image plane, we can then combine them to simulate what our square-law detector would see, the intensity pattern. The result is then Fourier transformed to see the individual conjugate components that make up the field, as shown in Figure 3-3. In this space we can clearly see the circular pupils caused by convolving our target with the pupil function's transform.

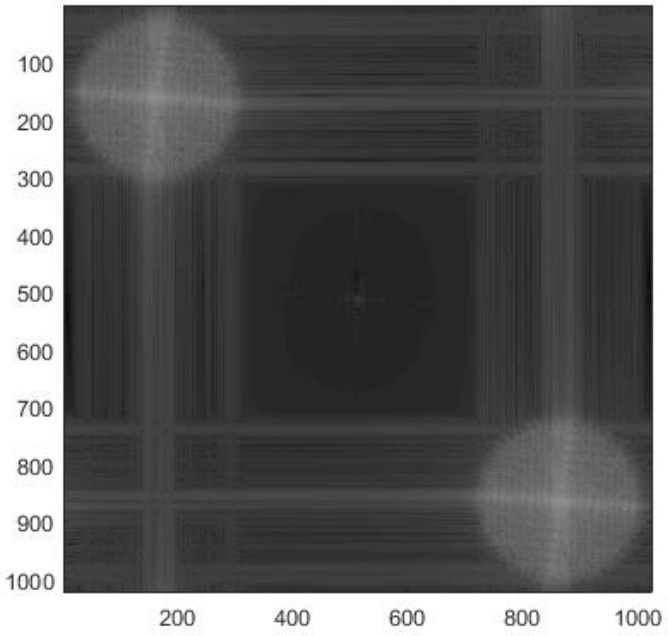

Figure 3-3: Fourier Plane from Intensity Image

One of the pupils is then chosen based on the LO shift, which determines which contains the conjugate image field or the original image field, and is cropped out and re-centered in its plane. This removes the tilt caused by the angle between the LO and optical axis, as described previously. The cropped pupil is then inverse Fourier transformed back to the image space to retrieve the object and LO fields overlaid, the real portion shown in Figure 3-4. Taking the modulus squared, we get back the image of our object, shown in Figure 3-5.

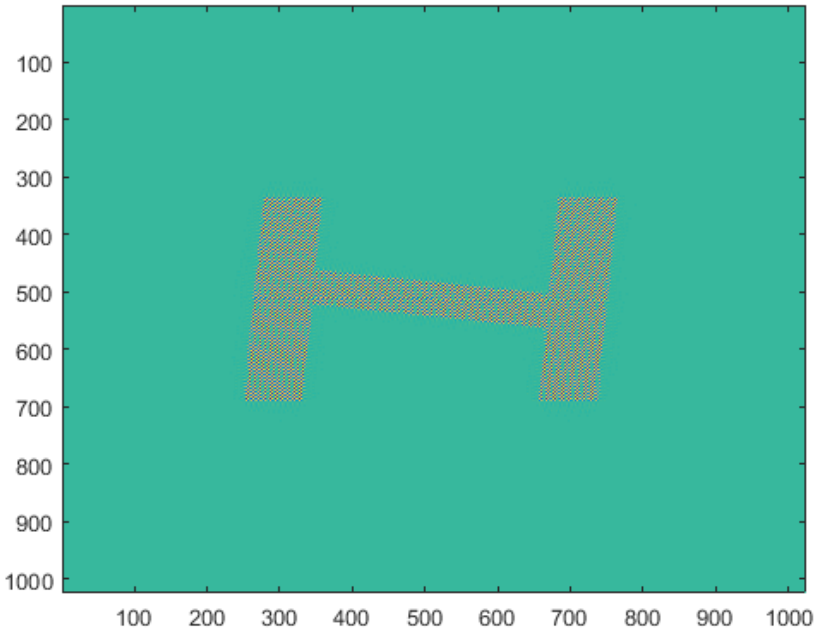

Figure 3-4: Object and LO Fields Retrieved from Fourier Plane

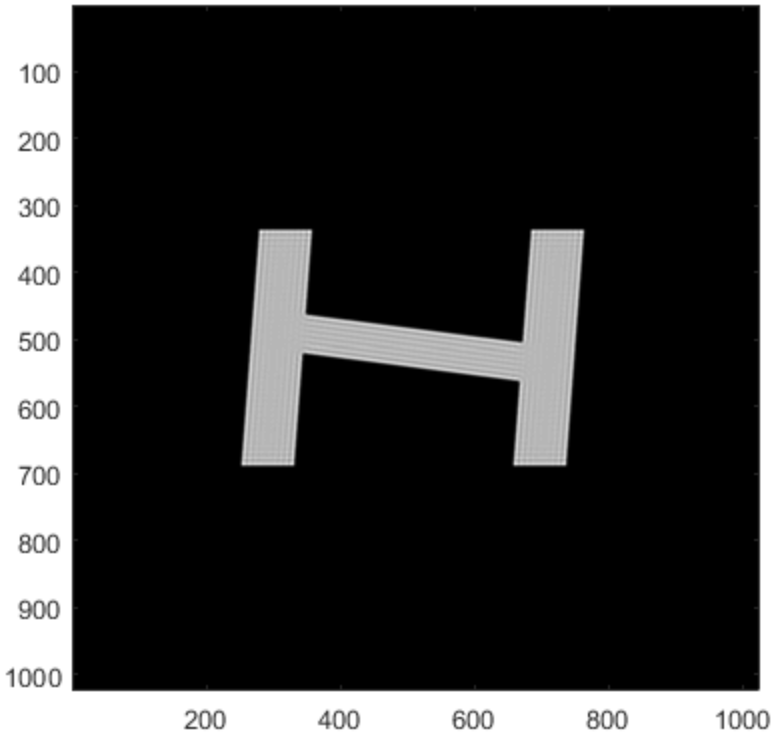

Figure 3-5: Intensity of Fields Showing Reconstructed Object Shape

3.2 Spatial Heterodyne with PRBS Modulation

Since we have shown that our system is successful in retrieving the object field from the pupil we can begin the portion of the simulation where the phase of the original LO and object fields are modulated according to a PRBS. We will use an array of PRBS patterns to show the effects of each; PRBS4, 7 & 9 are the sequences we will use. As the sequences get longer the simulation time takes an exponentially greater period of time to run, so the results will be trimmed, but will show a consistent pattern.

Two functions were created for the author's own benefit to find each MLS given a certain shift-register length. The first sequence generated by each length (the choice does not affect the results, as they are functionally equivalent) and imported into a vector in the

script. The code for the sequence generation in given in Appendix A. The sequence being analyzed is then stretched by a factor of 10 so that sub-bit shifts can be more easily performed. This takes a PRBS4 pattern, which would originally be 15 bits in length, to 150; or a PRBS9 pattern of 511 bits to 5110.

In order to simulate the length of code that will impact the signal during the camera's integration time, 0.5 ms, we repeat the code several times during our simulation length, but we will show this does not have any effect due to the autocorrelation properties of a PRBS sequence. Iterating over a non-integer multiple of the PRBS sequence, or stopping in mid-sequence has limited effect that degrades our isolation, but only in the limit of a few sequences. Any integration time that is many code lengths long will suffice. For instance, our camera integration time of 0.5 ms would see almost 197 repetitions for a PRBS7 pattern modulated at 50 MHz. This effect will be discussed later.

Since we have already calculated the LO field at the image plane, we need only multiply that result by a constant phase of 0 or pi to represent the two binary states of our phase modulator. The same will be done for the object field at the image plane. The script must then iterate and decide each time which state of each field it will combine. Figure 3-6 depicts the phase states of the two fields and the resulting phase difference for each 0.1 bit point in the sequence, using no mismatch between the two, which results in a constant phase difference throughout. We then take the intensity (magnitude squared) of the object and LO fields (as they would be seem on the camera) and then sum them into a matrix comprised of the previous iterations. The process loop is depicted in Figure 3-9.

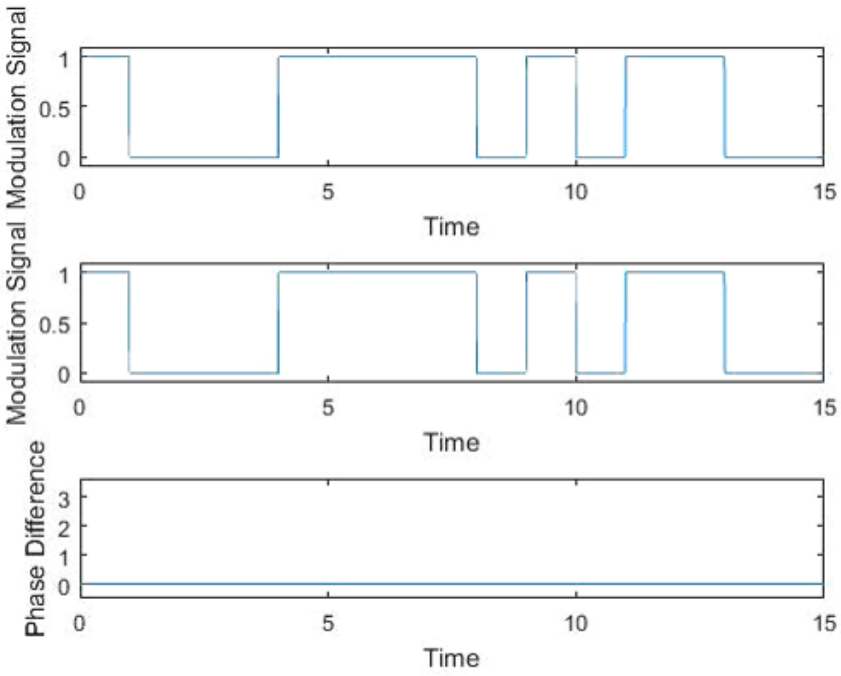

Figure 3-6: Object and LO Phase Modulation and Phase Difference w/no Offset

To create the next phase offset, the script can shift the mismatch in the signal and LO codes by 0.1 bit. We are interested to see that the theory of the autocorrelation of PRBS matches with the simulation. Once we increase the offset shift, the code runs through the math again and recalculates the intensity image that the camera sees. This process can be repeated for an entire sequence, but takes double the amount of time for every added bit, as expected. Figure 3-7 and Figure 3-8 depict the phase mismatch for both an offset less than one bit and for an offset greater than one bit, respectively. Notice that the duty cycle of the phase difference becomes approximately 50% when the offset is greater than one bit, this reduces the heterodyne efficiency and gives greater isolation with longer codes, as the duty cycle approaches the 50% limit. The cartoon is not a MLS PRBS and should not be taken literally, but is representative of the process.

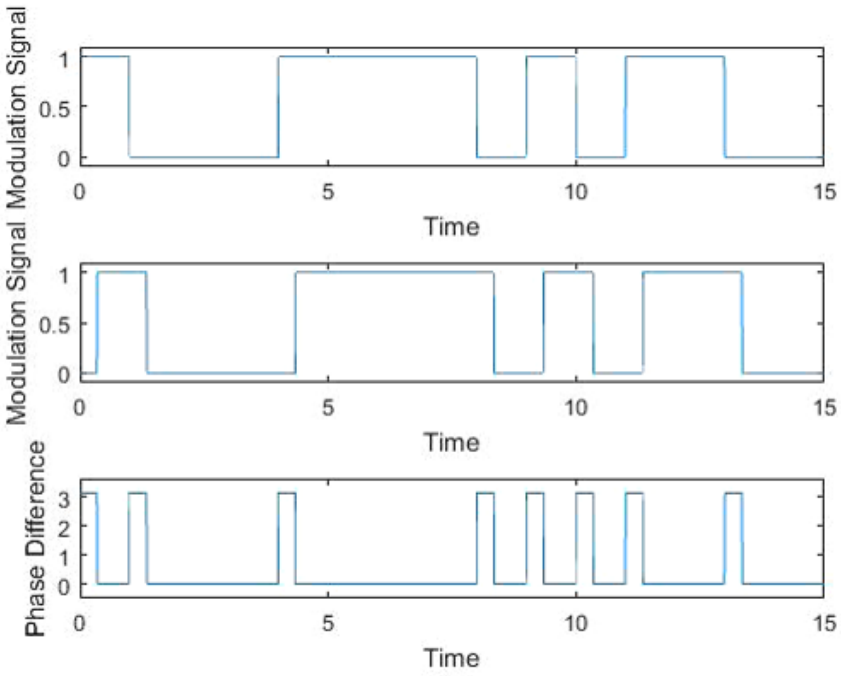

Figure 3-7: Object and LO Phase Modulation and Phase Difference w/Less than 1 Bit Offset

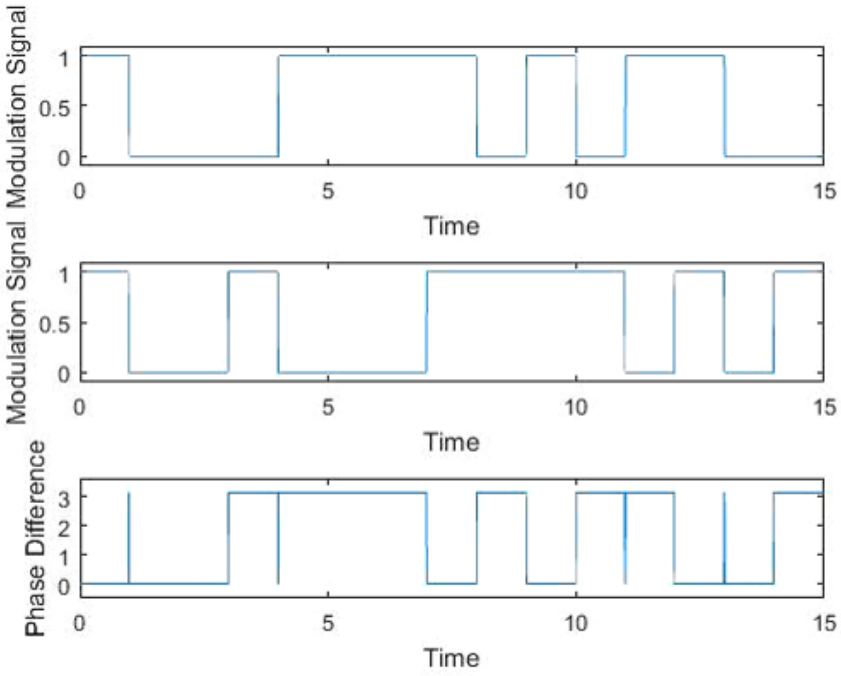

Figure 3-8: Object and LO Phase Modulation and Phase Difference w/Greater than 1 Bit Offset

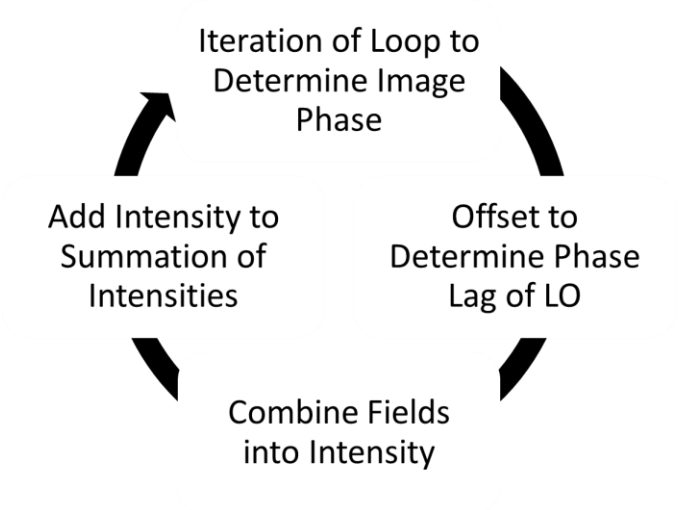

Figure 3-9: Iterative Loop to Simulate PRBS Modulated System

Once the process is completed we have one image comprised of the individual images of a full PRBS. We use the previous process described in the simpler spatial heterodyne section to find the intensity in the pupil, and sum the values in both dimensions to get a relative power number. Taking the 0 bit offset case as our standard (where the autocorrelation in PRBS is unity), we calculated the dB isolation from the standard as

$$dB\ power = 10 * log_{10}\left(\frac{Offset\ Power}{Standard\ Power}\right) \tag{3.3}$$

The results for some of the PRBS4 case are listed in Table 3-1. They are also truncated as the middle values (between 1 and 14 bit lag shift) are identical results. We put the Total Power field in the table to show that the total energy in the image does not change, but the phase modulation causes temporal fringes in mismatched code. This creates a DC term on our detector, the energy of which stays in the center of the Fourier plane.

Table 3-1: Power in Image and from Pupil Region in PRBS4 Case

Bit Shift	0	0.2	0.5	0.8	1	14	14.5
Total Power	1.39E+20	1.39E+20	1.39E+20	1.39E+20	1.39E+20	1.39E+20	1.39E+20
Pupil Power	1.51E+21	9.34E+20	3.29E+20	3.25E+19	6.71E+18	6.71E+18	3.29E+20
dB from Standard	0	-2.08	-6.62	-16.7	-23.5	-23.5	-6.62

The entire range of results is shown in Figure 3-10.

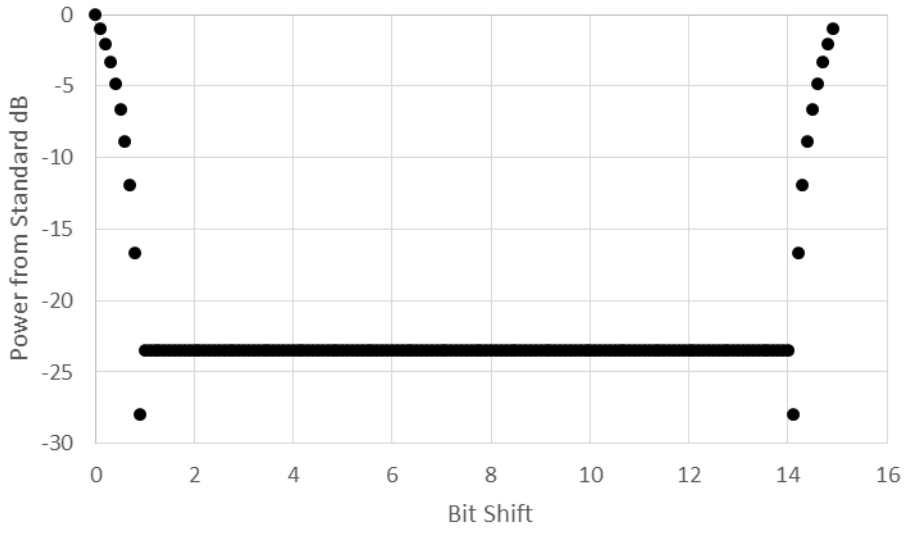

Figure 3-10: Power vs. Standard in Pupil Region in PRBS4 Case

The maximum power isolation achievable for a PRBS4 sequence is -23.52 dB, and so we see our simulation matches the theoretical value of the autocorrelation power of PRBS sequence,

$$dB\ power(PRBS) = 10 * log_{10}\left(\frac{1}{Length(PRBS)^2}\right). \quad (2.59)$$

The next case is for PRBS7, and a similar table and figure are shown below in Table 3-2 and Figure 3-11.

Table 3-2: Power in Image and from Pupil Region in PRBS7 Case

Bit Shift	0	0.2	0.5	0.8	1	126	126.5
Total Power	1.18E+21	1.18E+21	1.18E+21	1.18E+21	1.18E+21	1.18E+21	1.18E+21
Pupil Power	1.08E+23	6.90E+22	2.66E+22	4.06E+21	6.71E+18	6.71E+18	2.66e+22
dB from Standard	0	-1.96	-6.09	-14.3	-42.1	-42.1	-6.09

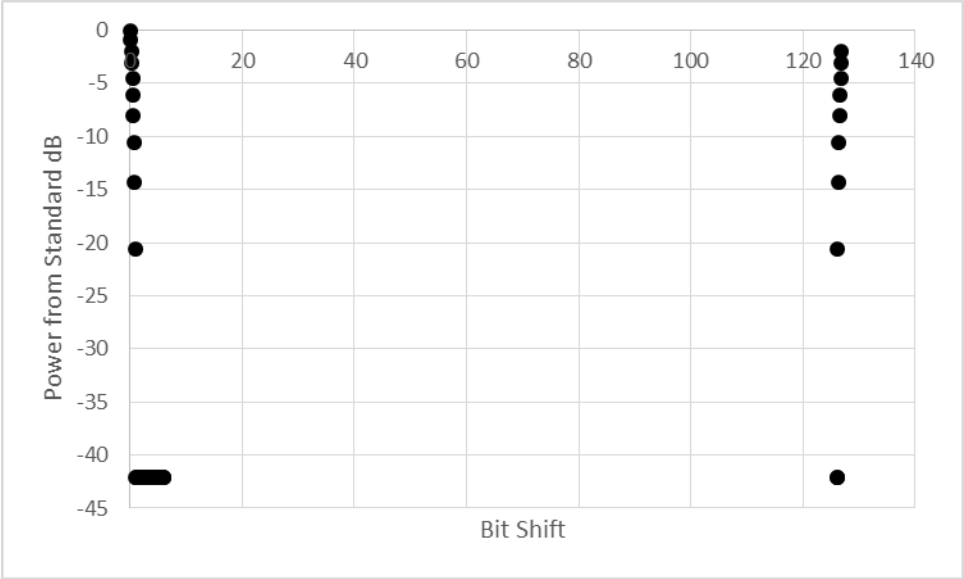

Figure 3-11: Power vs. Standard in Pupil Region in PRBS7 Case

The maximum achievable isolation using PRBS7 is -42.08 dB, which mirrors our simulation.

The last case we observe is the PRBS9 sequence. The length of the sequence is 511 bits, and the maximum isolation is -54.2 dB. Table 3-3 and Figure 3-12 show the results from this partial simulation.

Table 3-3: Power in Image and from Pupil Region in PRBS9 Case

Bit Shift	0	0.2	0.5	0.8	1	510	510.5
Total Power	4.73E+21	4.73E+21	4.73E+21	4.73E+21	4.73E+21	4.73E+21	4.73E+21
Pupil Power	1.75E+24	1.12E+24	4.36E+23	6.90E+22	6.71E+18	6.71E+18	4.36E+23
dB from Standard	0.00E+0	-1.94E+0	-6.04E+0	-1.40E+1	-5.42E+1	-5.42E+1	-6.04E+0

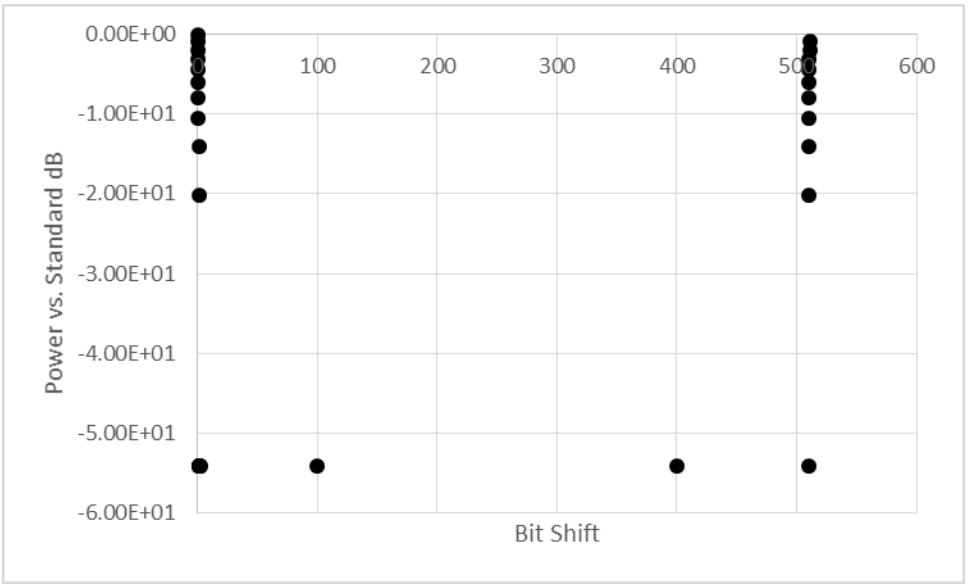

Figure 3-12: Power vs. Standard in Pupil Region in PRBS9 Case

3.3 Spatial Heterodyne with Truncated PRBS Modulation

The last piece to explore in the simulation is whether or not the real world case of a truncated PRBS pattern has any effect on the image. We anticipate that the more complete PRBS patterns the camera captures during its integration time, the less affected it is by the partial length of code (if there is one) that does not complete its sequence. If we imagine a truncated PRBS (that is not maximum length), we know it will not have the same autocorrelation isolation as the MLS version. Therefore, it stands to reason that if we have one full sequence and add the same truncated sequence to the end of it, the total sequence will have less isolation than the single sequence.

We model this effect by using our MATLAB script as previously done, but we change the conditions of the loop such that it stops before a full integer of sequence iterations. Using the PRBS4 sequence, Figure 3-13 shows the isolation of power vs. the standard 0-bit offset case for a variety of offset values. Each bit offset value was evaluated for various lengths of complete sequences added to a truncated sequence of 6 bits.

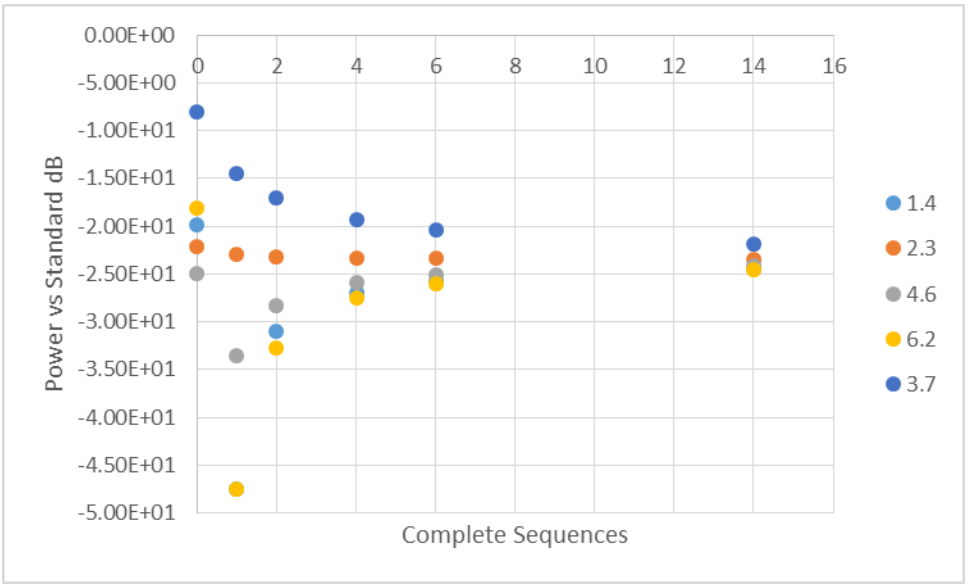

Figure 3-13: Power Isolation from Incomplete Sequences for Various Bit Shifts

As we added more complete PRBS4 sequences to the beginning of the code, the trends of each shift series converged on the autocorrelation limit for PRBS4. This test shows that as we integrate over many complete sequences, the addition of an incomplete sequence does not disrupt our power isolation significantly. This alleviates any doubts about running this without a triggering mechanism between the AWG and camera, although such a system can be implemented. Instead, we can have a free-running generator and capture frames at any period in time without much variance. If we consider the camera integration time intended to be used in the experiment, 0.5 ms, we see that even for our slowest repeating code and modulation, PRBS9 at 50 Mbit/s, we would receive 48 full code-lengths during the integration time. This alleviates much of the variance caused by the truncated sequence.

CHAPTER 4

EXPERIMENTAL RESULTS

4.1 Lab Setup

The experimental setup in the lab is shown in Figure 4-1. The laser used is a Cobolt Samba with a center frequency of 532.1±0.3 nm and a spectral linewidth (FWHM) of <1 MHz. The phase modulation was performed by a Tektronix 5014C AWG that fed a Conoptics Model 550 linear amplifier that drove their 360 series low-voltage phase modulator. The linear amplifier had bandwidth exceeding 300 MHz. The Tektronix AWG had predefined PRBS7 & 9 patterns, so none had to be loaded into the device, and could modulate them at a rate exceeding the limit of the amplifier.

The system was laid out in a manner consistent with Figure 4-1.

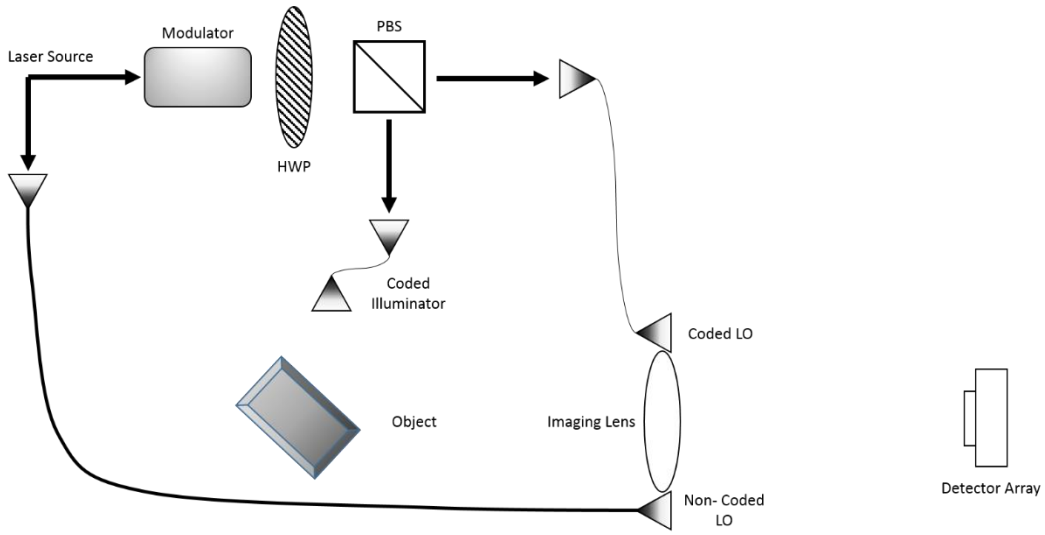

Figure 4-1: Optical Component Table Layout

The laser source was split into two paths using a half-wave plate (HWP) and polarization beam-splitter (PBS); one path of the laser source was directed into the phase modulator branch, the other was coupled into a fiber to serve as a CW LO. The modulator branch consisted of the Conoptics phase modulator, which was then passed through a HWP and PBS in order to better control the intensity of light directed at the target and camera, respectively. The fiber cables used were single-mode polarization maintaining fiber designed for our laser's wavelength of 532nm. The fiber tips were rotated such that the polarization of the light emitted from the tips was the same as that returning from the object.

The camera used was a PointGrey (now part of FLIR) Grasshopper3 model GS3-U3-23S6M-C. The camera is natively 1920 by 1200 pixels in format, but the active sensor area was reduced to the central 1024 by 1024 pixels. The cameras were managed through the NI MAX program, part of the LabVIEW suite, which allows full control of all the camera attributes. Shutter time, gain, gamma, black level, active sensor region, frame-rate, etc. could all be controlled through this application. Shutter speed, or exposure time, was set to 0.5 ms.

The object used was a chrome-on-glass mask of the ISO 12233 resolution target, of which we chose the region containing the slant “H” to image. Figure 4-2 is the entire mask and is the area of interest. Behind the mask was a metal plate with a rough surface. The target was oriented in such a manner that the specular reflection was not directly aimed back to the camera. Imaging was performed by a single positive, dual-convex lens set between the object and image planes. The lens was 2 inches in diameter and had a focal length of 1 meter for our wavelength.

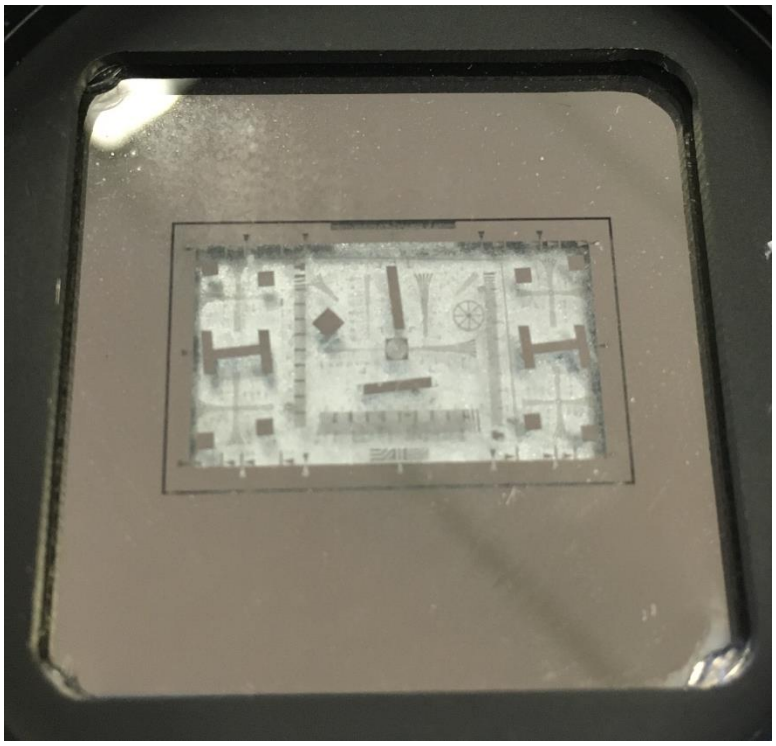

Figure 4-2: Image of Target Mask; Chrome on Glass Pattern

Figure 4-3: Mask Region of Interest

The images were collected using LabVIEW software; first, using a panel designed to quickly view the image data and its Fourier transform in real-time, then second, capturing images and storing them in .png format so as not to lose data to compression. Other formats could have been used, so long as they were lossless in format. A screenshot of the LabVIEW panel is shown in Figure 4-4 for reference.

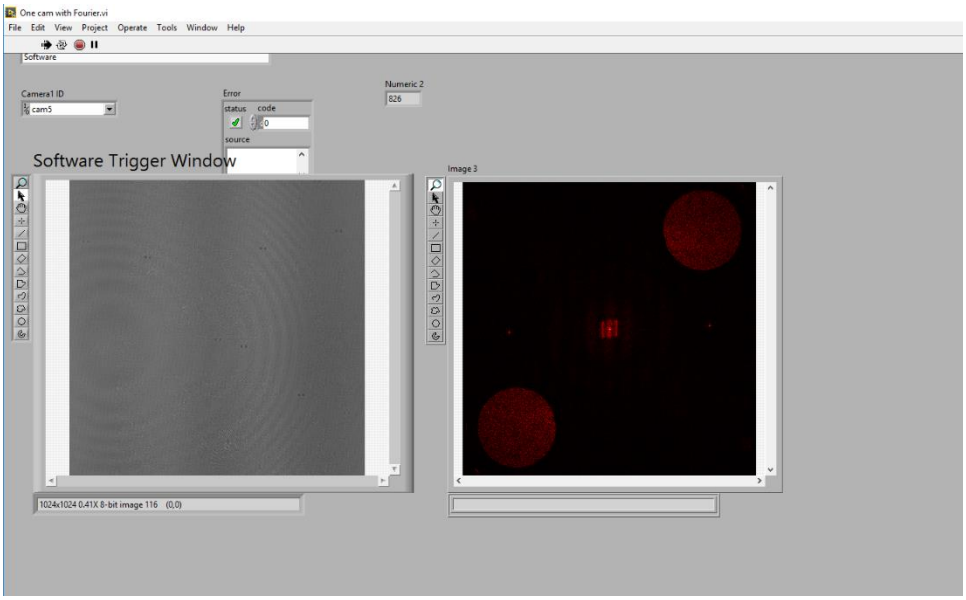

Figure 4-4: LabVIEW Panel of Image and Fourier Transform

Once the system was powered up and the laser sufficiently warmed-up the LabVIEW panel was run. The real-time Fourier view of the camera capture allowed for ease in balancing the powers in the two LOs and the signal, such that the pupils in all four quadrants were of equal brightness/contrast. The system was then set for the experiment and various cases of PRBS pattern length, modulation frequency, and optical path difference were tested. A single image for each instance was considered sufficient for the purposes of this project.

4.2 Data Collection

The first data taken were of the signal and two LOs where no modulation was applied. This is used as a reference point for the power levels in each area of the captured image: the entire image frame and one pupil each for the two corresponding LOs. A representative image captured by the camera is shown in Figure 4-5. The discontinuous striping in the figure is caused by the aliasing of the high spatial frequency fringes in the image being resized to this page. Figure 4-6 is an image of the Fourier plane of the fields with no modulation applied. The two sets of pupils can be seen to be nearly the same brightness.

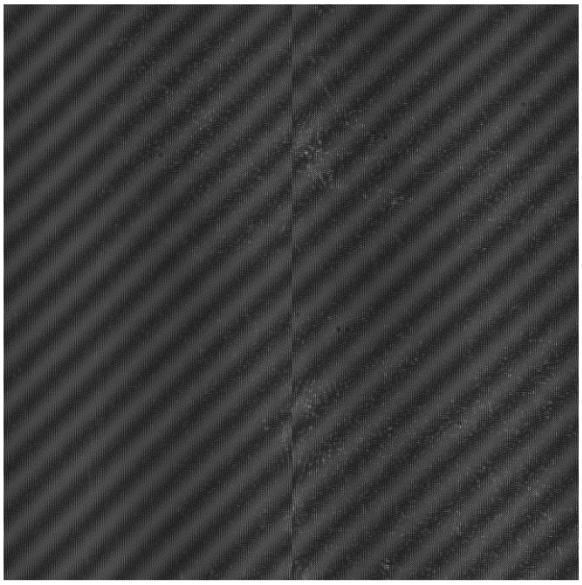

Figure 4-5: Representative Spatial Heterodyne Image Capture

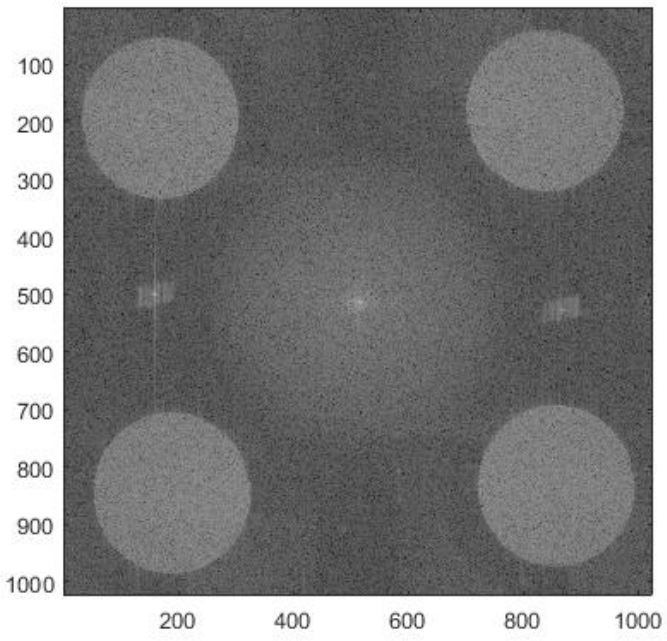

Figure 4-6: Fourier/Pupil Plane with No Modulation Applied

The same process is then followed as in the simulation; the pupils are cropped, a circle mask is applied, and they are inverse transformed back to the image plane, where

the power is calculated for each component. The calculated powers for the case with no modulation code is given in Table 4-1. The recovered image is shown in

Table 4-1: Powers from Section of Image with No Modulation

Full Image	PRBS Pupil	CW Pupil
6.15E+07	3.38E+07	3.37E+07

The next step was to apply a phase code to the signal beam and one of the LOs. The AWG was set to a PRBS7 (127 bit) pattern and modulated at 50, 100, 150, 200 & 300 Mbit/s. A representative image of the pupil plane is shown in Figure 4-7. Notice that one set of pupils is now greatly diminished in power. The recovered images of the “H” target from each the modulated and unmodulated LOs are given in Figs. 4-8 and 4-9 respectively. The calculated powers for each modulation rate are given in Table 4-2.

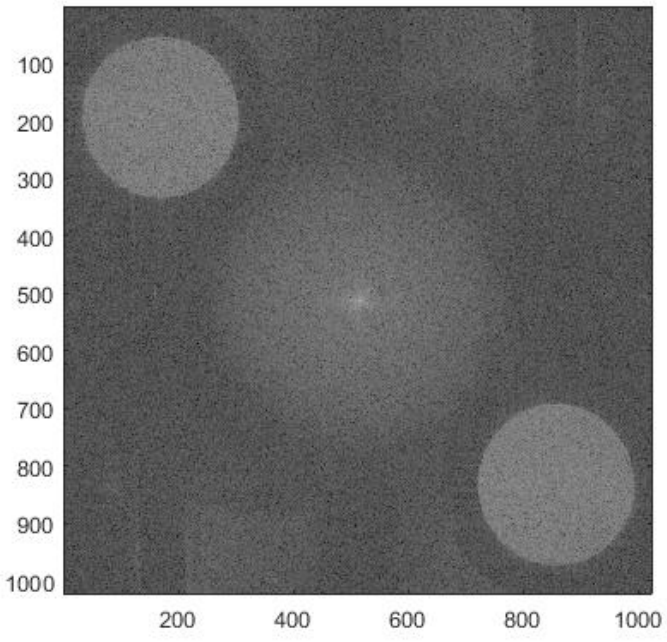

Figure 4-7: Fourier/Pupil Plane with PRBS7 Modulation Applied

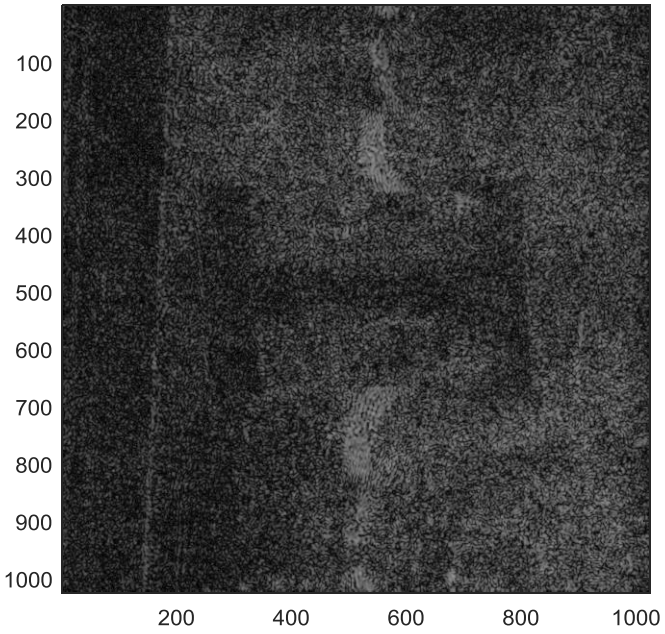

Figure 4-8: Recovered Image of "H" Target from Pupil Corresponding to Modulated LO

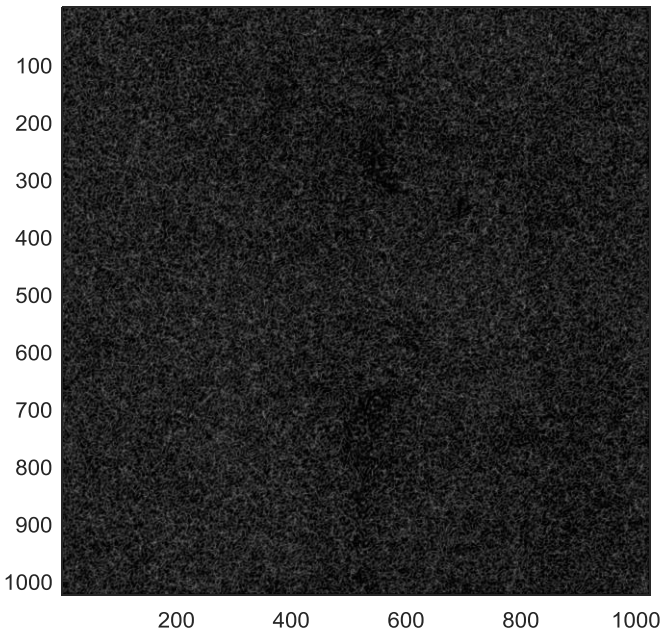

Figure 4-9: Recovered Image of "H" Target from Pupil Corresponding to Unmodulated LO

Table 4-2: Powers from Sections of Image with PRBS7 Modulation

	Full Image	PRBS Pupil	CW Pupil
50 Mbit/s	6.18E+07	2.78E+07	1.86E+06
100 Mbit/s	6.20E+07	2.43E+07	2.19E+05
150 Mbit/s	6.09E+07	1.84E+07	2.68E+05
200 Mbit/s	6.22E+07	1.88E+07	2.10E+05
300 Mbit/s	6.31E+07	1.70E+07	2.04E+05

The same was done for the PRBS9 case, with the results listed in

Table 4-3.

Table 4-3: Powers from Sections of Image with PRBS9 Modulation

	Full Image	PRBS Pupil	CW Pupil
50 Mbit/s	5.91E+07	2.41E+07	1.72E+06
100 Mbit/s	5.91E+07	1.93E+07	2.04E+05
150 Mbit/s	6.17E+07	2.01E+07	1.88E+05
200 Mbit/s	6.12E+07	1.65E+07	1.96E+05
300 Mbit/s	6.16E+07	1.67E+07	2.29E+05

To calculate the isolation achieved, we compare the modulated and unmodulated pupils. Table 4-4 reports the isolation achieved in dB for the PRBS7 and PRBS9 cases.

Table 4-4: dB Isolation Achieved Between Pupils

	PRBS7	PRBS9
50 Mbit/s	-1.17E+01	-1.15E+01
100 Mbit/s	-2.05E+01	-1.98E+01
150 Mbit/s	-1.84E+01	-2.03E+01
200 Mbit/s	-1.95E+01	-1.93E+01
300 Mbit/s	-1.92E+01	-1.86E+01

The last sets of data taken were for the various lengths of fiber added to the coded LO path to create a large OPD. This was to simulate returns from objects at distances where the phase codes do not align, in order to show isolation in imaging such objects. The various path length differences and the modulation rate results are given in Table 4-5, Table 4-6, and Table 4-7.

.

Table 4-5: Powers from Sections of Image with PRBS7 Modulation and 3m Fiber Length

	Full Image	PRBS Pupil	CW Pupil
50 Mbit/s	6.02E+07	2.42E+06	1.72E+06
100 Mbit/s	5.95E+07	1.25E+05	1.25E+05
150 Mbit/s	5.84E+07	1.23E+05	1.82E+05
200 Mbit/s	6.06E+07	1.29E+05	1.24E+05
300 Mbit/s	5.97E+07	2.77E+05	1.16E+05

Table 4-6: Powers from Sections of Image with PRBS7 Modulation and 9m Fiber Length

	Full Image	PRBS Pupil	CW Pupil
50 Mbit/s	5.85E+07	1.11E+05	1.65E+06
100 Mbit/s	5.82E+07	1.70E+05	1.21E+05
150 Mbit/s	5.67E+07	1.19E+05	1.78E+05
200 Mbit/s	5.81E+07	1.18E+05	1.19E+05
300 Mbit/s	5.85E+07	3.28E+05	1.16E+05

Table 4-7: Powers from Sections of Image with PRBS7 Modulation and 12m Fiber Length

	Full Image	PRBS Pupil	CW Pupil
50 Mbit/s	8.74E+07	3.18E+05	1.02E+06
100 Mbit/s	8.62E+07	1.07E+06	1.69E+05
150 Mbit/s	8.43E+07	1.48E+05	1.84E+05
200 Mbit/s	8.74E+07	7.39E+05	1.65E+05
300 Mbit/s	8.82E+07	1.92E+05	1.60E+05

To calculate the isolation achieved by the OPD mismatch, we compare each PRBS pupil from each of the fiber lengths against the standard values given in Table 4-2, again for each modulation frequency. The results are given in Table 4-8.

Table 4-8: Isolation Achieved by OPD between Signal and LO Paths

	3m Difference	9m Difference	12m Difference
50 Mbit/s	-1.06E+01	-2.40E+01	-1.94E+01
100 Mbit/s	-2.29E+01	-2.15E+01	-1.36E+01
150 Mbit/s	-2.18E+01	-2.19E+01	-2.10E+01
200 Mbit/s	-2.16E+01	-2.20E+01	-1.41E+01
300 Mbit/s	-1.79E+01	-1.71E+01	-1.95E+01

The results of this experiment are clear, we have achieved isolation of the signal from our noise by both un-coded returns through our imaging system and returns that exhibit an optical path difference greater than the “wavelength” of the modulation frequency of the code. If we closely examine the 3 meter fiber case in Table 4-8, we notice that the isolation is much less at 50 Mbit/s than at and other bit rate. This is because the length a bit takes travelling in space at that modulation frequency is 6 meters and, therefore, the OPD is not quite great enough to bring the autocorrelation of the PRBS to its lowest threshold.

We also notice that, for these PRBS7 & 9 cases, we are not achieving the maximum results that our simulation predicted. This can be caused by several reasons. Observations while doing setups for other experiments noted that the polarization in the fibers seems to wander while they settle after being moved around, which may cause some lowering of efficiency. Also, since the additional fiber lengths were butt-coupled in, we expect decent efficiency of power transfer at each junction, but we also see that it can affect total image power, as shown in Table 4-7 compared to the two previous to it. Even though great care was taken during setup, the optical path lengths may have also been slightly off, which has been shown previously to cause large efficiency effects, even within one bit-length of offset.

CHAPTER 5

CONCLUSION

5.1 Simulation Conclusion

The simulation was successful in showing that spatial heterodyne imaging is possible in the presence of PRBS phase modulation. Not only does it show that we can perform this imaging, but we can achieve isolation of our targets with respect to their surrounding if our imaging system has a large enough depth of focus. We have also shown that the isolation provided is relatively independent of the modulation frequency of the PRBS sequence when we have many sequences incident during the camera's integration period. The isolation available is dependent of the length of the pattern and is given in Eq. (3.3).

5.2 Experimental Conclusion

The experiment conducted was successful in showing, in real-time and through image processing, that the mixing efficiency of the signal and LO could be greatly affected through PRBS phase modulation. By modulation with different lengths of code, we had hoped to achieve better results for the longer length (PRBS9) code, but ultimately we seemed to be limited by our equipment and setup practices. We did show that by mismatching the optical path lengths between two modulated branches of our system we simulate changing the distance to our target. This allowed us to follow the simulation, laid

out previously, and misalign the codes at the imaging plane, creating temporal fringes and reducing heterodyne efficiency.

5.3 Future Work

It would be beneficial to design a better imaging system with a large depth of focus so we can run the experiment again with multiple targets separated in distance along the optical axis. This would better show the effectiveness of this method at isolating targets in distance with respect to the code length and modulation frequency. The SNR of the camera should also be taken into consideration, as the isolation values we are hoping to achieve may be much greater than the camera's sensitivity and dynamic range is capable of. Additionally, as we modulate to higher bit rates we should be able to "focus" our system to finer distance resolutions. This would mean creative methods for controlling the focus, such as dynamically changing the optical path length or the modulation frequency, pattern, and phase delay. This could be done with two phase modulators linked to an AWG that allows a temporal shift between the two driving signals. The theory required to create such systems should largely be covered in this thesis.

It would be very useful to employ this imaging approach while viewing an object embedded in a cloud chamber. Embedding the target in a cloud chamber will allow us to determine how well this imaging approach will work for objects embedded in obscurants.

REFERENCES

[1] R. L. Bobb, “[Thesis] Dopplar Shift Analysis For A Holographic Aperture LADAR System,” 2012.

[2] E. N. Leith and J. Upatnieks, “Reconstructed Wavefronts and Communication Theory,” *J. Opt. Soc. Am.*, vol. 52, no. 10, p. 1123, 1962.

[3] E. N. Leith and J. Upatnieks, “Wavefront Reconstruction with Continuous-Tone Objects,” *J. Opt. Soc. Am.*, vol. 53, no. 12, pp. 1377–1381, 1963.

[4] E. N. Leith and J. Upatnieks, “Wavefront Reconstruction with Diffused Illumination and Three-Dimensional Objects,” *J. Opt. Soc. Am.*, vol. 54, no. 11, pp. 1295–1301, 1964.

[5] D. Gabor, “A New Microscopic Principle,” *Nature*, vol. 161, no. 4098. pp. 777–778, 1948.

[6] J. W. Goodman, “DIGITAL IMAGE FORMATION FROM ELECTRONICALLY DETECTED HOLOGRAMS,” *Appl. Phys. Lett.*, vol. 11, no. 77, 1967.

[7] F. J. MacWilliams and N. J. A. Sloane, “Pseudo-random sequences and arrays,” *Proc. IEEE*, vol. 64, no. 12, pp. 1715–1729, 1976.

[8] D. A. Shaddock, “Digitally Enhanced Heterodyne Interferometry,” *Opt. Lett.*, vol. 32, no. 22, pp. 3355–7, 2007.

[9] G. de Vine, D. S. Rabeling, B. J. J. Slagmolen, T. T.-Y. Lam, S. Chua, D. M. Wuchenich, D. E. McClelland, and D. A. Shaddock, “Picometer level displacement metrology with digitally enhanced heterodyne interferometry.,” *Opt. Express*, vol. 17, no. 2, pp. 828–837, 2009.

[10] J. W. Goodman, *Introduction to Fourier Optics*, Third. Roberts & Company Publishers, 2005.

[11] J. Kraczek, “[Thesis] Piston Phase Measurements to Accelerate Image Reconstruction in Multi-Aperture Systems,” no. December, 2011.

APPENDIX A

Spatial Heterodyne Simulation Code (MATLAB)

```
%Spatial Heterodyne Simulation with Pseudo Random Bit Sequence
%James Zimnicki
%University of Dayton

%The purpose of this code is to simulate the spatial heterodyne mixing
%of a object ('target') return field with that of a local oscillator.
%Phase modulation is applied via a PRBS


target = imread('target_shape.png'); %Load Object Image
target_field = sqrt(im2double(target(:,:,1))); %SQRT to simulate 'field' from
%intensity image


%Create system variables and constants
lambda = 0.000000532;   %Set to source wavelength
k = 2*pi/lambda;    %wavenumber from lambda
z3 = 2;     %Propagation distance from LO to Image plane
c = 3.0E8;  %Speed of light in m/s

pp = 0.00000586; %Pixel Pitch of detector
pixel = 1024; %# of pixels used in each dimension
diam = pixel*pp;     %Diameter of detector array, Pixel pitch * # of pixels

%Set the number of iterations to loop through, offset will increase by one
%tenth bit for every iteration.
iter = 1;
iter_offset = 0;%starting offset (tenth of bits)
truncate = 0;%how many tenth of bits to truncate from the end of PRBS


%Create the PRBS for various lengths. Can leave uncommented or commented
%without affecting speed of simulation much.
n7 = [1,0,0,0,0,0,0,1,1,1,1,1,1,1,0,1,0,1,0,1,0,0,1,1,0,0,1,1,1,0,1,1,...
    1,0,1,0,0,1,0,1,1,0,0,0,1,1,0,1,1,1,1,1,0,1,1,0,1,0,1,1,0,1,1,0,0,1,...
    0,0,1,0,0,0,1,1,1,0,0,0,0,1,0,1,1,1,1,1,1,0,0,1,0,1,0,1,1,1,0,0,1,1,...
    0,1,0,0,0,1,0,0,1,1,1,1,0,0,0,1,0,1,0,0,0,0,1,1,0,0,0,0,0];
n3 = [1,     0,     0,     1,     1,     1 ,    0];
n4 = [1,0,0,0,1,1,1,1,0,1,0,1,1,0,0];
```

```
% n9 = [1,0,0,0,0,0,0,0,0,1,0,0,0,1,0,0,0,1,1,0,0,1,0,0,0,1,1,1,0,1,0,...
%     1,0,1,1,0,1,1,0,0,0,1,1,1,0,0,0,1,0,0,1,0,1,0,1,0,0,0,1,1,0,1,1,...
%     0,0,1,1,1,1,1,0,0,1,1,1,1,0,0,0,1,0,1,1,0,1,1,1,0,0,1,0,1,0,0,1,...
%     0,0,0,0,0,1,0,0,1,1,0,0,1,1,1,0,1,0,0,0,1,1,1,1,1,0,1,1,1,1,0,0,...
%     0,0,0,1,1,1,1,1,1,1,1,1,0,0,0,0,1,1,1,1,0,1,1,1,0,0,0,0,1,0,1,1,...
%     0,0,1,1,0,1,1,0,1,1,1,1,0,1,0,0,0,0,1,1,1,0,0,1,1,0,0,0,0,1,0,0,...
%     1,0,0,0,1,0,1,0,1,1,1,0,1,0,1,1,1,1,0,0,1,0,0,1,0,1,1,1,0,0,1,1,...
%     1,0,0,0,0,0,0,1,1,1,0,1,1,1,0,1,0,0,1,1,1,1,0,1,0,1,0,0,1,0,1,0,...
%     0,0,0,0,0,1,0,1,0,1,0,1,0,1,1,1,1,1,1,0,1,0,1,1,0,1,0,0,0,0,0,1,1,...
%     0,1,1,1,0,1,1,0,1,1,0,1,0,1,1,0,0,0,0,0,0,1,0,1,1,1,0,1,1,1,1,1,0,...
%     0,0,1,1,1,1,0,0,1,1,0,1,0,0,1,1,0,1,0,1,1,1,0,0,0,1,1,0,1,0,0,0,...
%     1,0,1,1,1,1,1,1,1,0,1,0,0,1,0,1,1,0,0,0,1,0,1,0,0,1,1,0,0,0,1,1,...
%     0,0,0,0,0,0,0,1,1,0,0,1,1,0,0,1,0,1,0,1,1,0,0,1,0,0,1,1,1,1,1,1,...
%     0,1,1,0,1,0,0,1,0,0,1,0,0,1,1,0,1,1,1,1,1,1,1,0,0,1,0,1,1,0,1,0,1,...
%     0,0,0,0,1,0,1,0,0,0,1,0,0,1,1,1,0,1,1,0,0,1,0,1,1,1,1,0,1,1,0,0,...
%     0,0,1,1,0,1,0,1,0,1,0,0,1,1,1,0,0,1,0,0,0,0,1,1,0,0,0,1,0,0,0,0];


c_t = linspace(1, 10*length(n4), 10*length(n4)); %vector sized 10x code
%                                                 length
phase_code = c_t; %placeholder variable to be changed

%This loop "stretches" the PRBS to take up 10 bits for each bit
%Which will be used for sub-bit shifting
for a = 1:length(c_t)
   phase_code(a) = n4(ceil(c_t(a)/10));
end

phase_code_long = repmat(phase_code,1,2);%Repeat code by the last integer
%to simulate multiple lengths during a camera integration time. The number
%of full codes is N-1-(tuncate/length(phase_code)). This should be set to
%at least 2.


%Create vectors with spacing based upon the pixel pitch of the camera
u = linspace(0,diam,pixel);
v = linspace(0,diam,pixel);

a_lo = -0.0254; %distance between LO and horizontal axis
b_lo = -0.0254; %distance between LO and vertical axis

%This loop calculates the field of the LO incident on the detector
%through Fresnel propagation.
for m = 1:length(u)
   for n = 1:length(v)
      lo_field(m,n) = exp((1i*k/(2*z3))*(u(m)^2 + v(n)^2))*...
         (exp(1i*k*z3)/(1i*lambda*z3))*...
         exp((1i*k/(2*z3))*(a_lo^2 + b_lo^2))*...
         exp(-(1i*k/(z3))*(u(m)*a_lo + v(n)*b_lo));
   end
end
```

```
%These are the two fields we are concerned with, one with no phase
%shift and the second with pi phase shift. We need only generate these
%once.
lo_field0 = lo_field*exp(1i*0);
lo_fieldpi = lo_field*exp(1i*pi);
lo_fields = zeros(1024,1024,2); %array to store both LO fields
lo_fields(:,:,1) = lo_field0; %sub-matrix to store LO w/no shift
lo_fields(:,:,2) = lo_fieldpi; %sub-matrix to store LO w/pi shift


%Circle mask for lens pupil to simulate the PSF of the system.
center_x=512;center_y=512;size_x=1024;size_y=1024;r=128;
[x_mesh,y_mesh]=meshgrid(-(center_x-1):(size_x-center_x),...
    -(center_y-1):(size_y-center_y));
c_mask=((x_mesh.^2+y_mesh.^2)<=r^2);


%Takes the Fourier of the object and multiplies by the mask. The same
%operation as convolution in the transformed space, but faster in
%implimentation
target_ft = fftshift(fft2(target_field,1024,1024));
target_field_mask_ft = c_mask.*target_ft;
target_field_masked = (ifft2(target_field_mask_ft,1024,1024));


%Various placeholder matrices
target_code = zeros(length(u),length(v));
im_intensity = zeros(length(u),length(v));
im_power = zeros(1,iter);
pupil_power1 = zeros(1,iter);
pupil_power2 = zeros(1,iter);
```

```
%%%%%%%%%%%%%%%%%%%%%%%%%%%%%%%%%%%%%%%%%%%%%%%%%%%%%%%%%%%%%%%%%%%%%%%%
%Main iterative loop
% tic
for d =1:iter %loops through and increases offset by 1/10 bit each time


   code_delay = iter_offset + d-1;%sets the number of bits to offset by
   %and adjusts each iteration

   %This loop takes the target and LO fields, adds in the appropriate
   %phase to each field, then takes the intensity. The loop is iterated
   %through the number of code lengths the user has chosen above. This
   %simulates all the phase combinations present on the detector during
   %the integration period.
   for a = 1:length(phase_code_long)-length(phase_code)-truncate
      target_code = target_field_masked*exp(1i*pi*phase_code_long(a));
      lo_field_code = lo_fields(:,:,phase_code_long(a+code_delay)+1);
      im_intensity = im_intensity + abs(lo_field_code + target_code).^2;



   %a handy percent counter, which is not too intrusive on speed.
%        percent_complete = (((a)/(iter*(length(phase_code_long)-...
%           length(phase_code)-truncate))) +(d-1)*(1/iter)) *100


   end



   %Sum all intensities in the image plane to get a relative power level
   im_power(1,d) = sum(sum((im_intensity)));

   %FFT of the total intensity image to get Fourier Plane
   im_ft = fftshift(fft2(im_intensity));

   %Can show Fourier Plane
%        figure()
%        imagesc(log10(abs(im_ft)))
%        colormap gray
%        axis image


   %Crop region associated with pupil. May need adjustment based on user
   %settings.
   im_crop = im_ft(1:322,1:322);
```

```
    %Creates a binary circle mask to crop only the pupil shape of
    %interest. May need resized and positioned for user's purposes.
    center_u=161;center_v=161;size_u=322;size_v=322;r2=160;
    [u_mesh,v_mesh]=meshgrid(-(center_u-1):(size_u-center_u),...
       -(center_v-1):(size_v-center_v));
    im_crop_mask=((u_mesh.^2+v_mesh.^2)<=r2^2);

    %Crop Pupil shape of interest
    im_crop = im_crop.*im_crop_mask;


    %Transform back to image plane
    im_restored = ifft2(im_crop,1024,1024);


    %Find power associated with Pupil Region of Fourier plane and plot
    %resulting intensity image after spatial heterodyne processing.
    pupil_power1(1,d) = sum(sum(abs(im_restored).^2));

%     figure()
%     imagesc(abs(im_restored).^2)
%     colormap gray
%     axis image


    %This section can be uncommented if the user is interested in seeing
    %that the second pupil contains similar information as the first, as it
    %is a conjugate image. The power levels should be equal if cropped
    %correctly.
    %     im_crop2 = im_ft(1024-321:1024,1024-321:1024);
    %
    %
    %     im_crop2 = im_crop2.*im_crop_mask;
    %
    %     im_restored2 = ifft2(im_crop2,1024,1024);
    %     pupil_power2(1,d) = sum(sum(abs(im_restored).^2));
    % %     figure()
    % %     imagesc(abs(im_restored2).^2)
    % %     colormap gray
    % %     axis image


%     toc
end%End of Iteration loop
```